2019

Novel coil designs for different neurological disorders in transcranial magnetic stimulation

Priyam Rastogi
Iowa State University

Novel coil designs for different neurological disorders in transcranial magnetic stimulation

by

Priyam Rastogi

A dissertation submitted to the graduate faculty

in partial fulfillment of the requirements for the degree of

DOCTOR OF PHILOSOPHY

Major: Electrical Engineering (Electromagnetics Microwave and Nondestructive Evaluation)

Program of Study Committee:
David Jiles, Major Professor
Jiming Song
Mani Mina
Long Que
Farzad Sabzikar

The student author, whose presentation of the scholarship herein was approved by the program of study committee, is solely responsible for the content of this dissertation. The Graduate College will ensure this dissertation is globally accessible and will not permit alterations after a degree is conferred.

Iowa State University

Ames, Iowa

2019

TABLE OF CONTENTS

LIST OF FIGURES

LIST OF TABLES

ACKNOWLEDGEMENT

I would like to thank my committee chair, Prof. David Jiles, and my committee members, Prof. Jiming Song, Prof. Mani Mina, Prof. Long Que, and Prof. Farzad Sabzikar, for their guidance and support throughout the course of this research.

Prof. David Jiles provided the opportunity for me to work on the biomedical research area, despite my little experience in the field of magnetics. I am eternally thankful to him for supporting me and guiding me throughout my research.

I would like to sincerely thank Prof. Ravi Hadimani at Virginia Commonwealth University, who guided and supported me throughout my research and several other tasks, starting from, when he was at Iowa State University. I would also like to thank Erik Lee whose insight knowledge and deep interest in TMS leads to innovative ideas and discussions which were essential to transform this research into a pioneering work. Yalun Tang, and Bowen Zhang were the most hard working undergraduate research assistants, and I wish them luck for their bright future.

Dr. Jayaprakash Selvaraj, my life partner who always motivated me and believed in me whenever I was in self-doubt and his endless encouragement to make my research successful. I would not have made this far without the love and constant support of my parents specially my mother Mrs. Jaishri Rastogi who stayed with me to complete this dissertation.

In addition, I would also like to thank my friends, colleagues, the department faculty and staff for making my time at Iowa State University a wonderful experience.

ABSTRACT

Transcranial magnetic stimulation is a non-invasive, safe, painless out-patient treatment for major depressive disorder. In TMS, time varying magnetic field is used to induce electric field, in the region of interest, to stimulate the neurons. Coil design is an important aspect of TMS, as coils are used to navigate the magnetic field in the desired location. The work presented in this dissertation is regarding the use of the coil design development for the application of transcranial magnetic simulation. Two TMS coils namely the Triple Halo Coil and the Quadruple Butterfly Coil were presented, with one aiming for deep brain stimulation and other one for precise stimulation. The magnetic field due to the Triple Halo Coil is 7 times more than circular coil at 10 cm below the head. It can stimulate deep brain regions which are affected in disorders such as Parkinson's disease and PTSD. The Quadruple Butterfly Coil has reduced volume of stimulation by around 10% at the vertex and dorsolateral prefrontal cortex when compared with the Figure-8 coil. Fifty heterogeneous MRI derived head models were used for the analysis of the induced electric field due to the Quadruple Butterfly Coil and the results were compared with the Figure-8 coil. For both the coils, first computer modelling was done on heterogeneous head models, using a finite element tool and testing using a prototype built by Jali Medicals with the help of an axial Hall probe and a gaussmeter. Furthermore, seven different coils for small animals were presented in this dissertation. These coils had varying electric field with the Slinky coil having the minimum area of stimulation and lowest electric field below 10 mm of the head, while the Animal Halo Coil had maximum area of stimulation and highest electric field at 1 mm below the head. Animal coils are important as animal testing reduces the cost and expedites the research time.

CHAPTER 1

INTRODUCTION

1.1 Overview of neurological disorders

According to the World Health Organization (WHO), one in every four persons in the world is or will be affected by neurological disorder at some point of their lives. Mental disorder is one of the leading causes of ill-health worldwide, contributing to approximately 450 million people suffering from this issue [1].

1.1.1 Mental illness

Mental illness can be classified into: Any Mental Illness (AMI) and Serious Mental Illness (SMI), which are defined below.

Any mental illness: "*Any mental illness (AMI) is defined as a mental, behavioral, or emotional disorder. AMI can vary in impact, ranging from no impairment to mild, moderate, and even severe impairment (e.g., individuals with serious mental illness).*" [2]

Serious mental illness: "*Serious mental illness (SMI) is defined as a mental, behavioral, or emotional disorder resulting in serious functional impairment, which substantially interferes with or limits one or more major life activities.*" [2]

National Survey on Drugs Use and Health (NSDUH) estimated that in 2016 in United States alone, 44.7 million adults (18.3%), over 18 years of age had AMI. AMI is found higher among women (27.7%) in comparison to men (14.5%). Younger population has the highest prevalence of AMI (18-25 years; 22.1%) when compared to middle aged (26- 49 years; 21.1%) and older populations (above 50 years; 14.5%). Although, only 43.1% (19.2 million) of the population who were diagnosed with AMI in 2016 received treatment. [2]

In 2016, 10.4 million adults (18.3%), over 18 years of age in United States had SMI. SMI is found higher among women (5.3%) in comparison to men (3%). Younger population has the highest prevalence of AMI (18-25 years; 5.9%) when compared to middle aged (26-49 years; 5.3%) and older population (above 50 years; 2.7%). Although, only 64.8% (6.7 million) of the population received treatment who were diagnosed with SMI in 2016. [2]

1.1.2 Major depression [2]

Major depression is one of the most common neurological disorder present in the United States. It can interfere with or limit the day to day activities of an individual. The definition of the major depression according to the NSDUH (National Survey on Drug Use and Health) is

"*A period of two weeks or longer during which there is either depressed mood or loss of interest or pleasure, and at least four other symptoms that reflect a change in functioning, such as problems with sleep, eating, energy, concentration, self-image or recurrent thoughts of death or suicide."* [2]

In 2016, 6.7% (16.2 million) of US adults aged 18 or older had at least one depressive episode. Females (8.5%) had higher prevalence of major depressive disorder in comparison to males (4.8%). It also had the highest prevalence for the age group between 18-25 affecting 10.9%.

Types of treatment for major depressive disorder includes treatment by (i) health professional alone, (ii) medication alone and (iii) both combined. 37% of adults with major depressive disorder did not received any treatment while 44% of adults received treatment with health professional and medication combined.

Major depressive disorder is also prevalent among adolescents. 3.1 million (12.8%) adolescents in United States within the age group of 12 to 17 years had at least one major depressive episode in 2016. Adolescent females (12.8%) had higher prevalence of major depression than in adolescent males (6.4%). Approximately, 60% of adolescents with major depression did not receive treatment while only 19% received combined health care by professionals and medications.

1.1.3 Schizophrenia [3]

Schizophrenia is another mental disorder which is among the top 15 leading causes of disability and its effects are devastating in the life of the patients and their loved ones. Schizophrenia is defined as *"schizophrenia is a mental disorder characterized by disruptions in thought processes, perceptions, emotional responsiveness, and social interactions. Although the course of schizophrenia varies among individuals, schizophrenia is typically persistent and can be both severe and disabling."*[3] Symptoms of schizophrenia are not limited to hallucinations, delusions, difficulty in social relationships, motor impairment, thought disorder, cognitive impairment (person having trouble in remembering, learning new things, making decisions), reduced expression of emotions and motivations toward goals.

Symptoms of schizophrenia typically starts in the early adulthood or late adolescence, typically in late teens and early thirties and continues to develop through time. Sometimes, cognitive impairment and unusual behaviors are seen during the childhood with the occurrence of more symptoms in the later stages. Furthermore, it tends to emerge earlier in males than females. Accurate estimation of schizophrenia patients is difficult, due to the complex nature of diagnosis, since it mostly overlaps with other mental disorders. In the United States, approximately 0.25% to 0.64% are affected by schizophrenia and other mental disorders.

Despite its relatively low prevalence, individuals affected with schizophrenia have higher premature mortality rates with the estimated potential life lost of 28.5 years (United States). Medical conditions such as diabetes, heart and liver diseases co-existing in schizophrenic patients, also contribute to the higher premature mortality rate. An estimated 4.9% patients affected with schizophrenia commits suicide, with the highest risk existing at the early stages of the illness.

1.1.4 Post-traumatic stress disorder (PTSD)[4]

Post-traumatic stress disorder (PTSD) is one of the most common mental illness among military veterans. It is defined as *"PTSD can develop after exposure to a potentially traumatic event that is beyond a typical stressor. Events that may lead to PTSD include, but are not limited to, violent personal assaults, natural or human-caused disasters, accidents, combat, and other forms of violence. People who experience PTSD may have persistent, frightening thoughts and memories of the event(s), experience sleep problems, feel detached or numb, or may be easily startled. In severe forms, PTSD can significantly impair a person's ability to function at work, at home, and socially."* [4]

In the year 2001-2003, 3.6% of adults (above 18 years) were diagnosed with PTSD in the United States, out of which 5.8% were females and 1.8% were males. Patients with life time prevalence of PTSD were found to be 6.8%. PTSD can be categorized into three levels from mild to serious based on the severity of impairment. The score for impairment is measured by Sheehan Disability Scale. It is estimated that 30.2% are affected with mild impairment, 33.1% with moderate impairment and 36.6% with serious impairment.

Estimated prevalence of PTSD among adolescents in the age group of 13-18 years is 5.0% with 1.5% of severe impairment. Adolescent females (8%) have higher prevalence of PTSD than males (2.3%).

1.1.5 Parkinson's disease [5]

Parkinson's disease (PD) is defined by "*as a neurodegenerative disorder, that is, a disease in which brain cells progressively die. Symptoms include tremor, rigidity, extreme slowness of movement, and impaired balance. Swallowing and speaking difficulties are also common, as are several non-motor symptoms that seriously affect quality of life.*" It is estimated that every year 50,000 people are diagnosed with PD and approximately half a million have this disorder in US alone. One of the symptoms of PD is the loss of nerve cells which releases dopamine, leading to the use of Levodopa drug which helps in reversing the symptoms of PD by increase in dopamine level. Furthermore, Levodopa cannot reverse the degenerations of the nerves, making it to be ineffective as the disease progresses, and it also has side effect named as dyskinesias in which there are uncontrolled movements.

DBS (deep brain surgery) is an invasive process in which the symptoms of PD are improved by electrically stimulating the nerves cell. In which, a stimulating electrode is placed deep inside the brain and a control device to control the amount of stimulation is placed in the chest. It also has several risks which includes surgery risks, side effects of stimulation such as balance problem, numbness, speech problems, and other side effects such as strokes, seizures, infection and confusion.

The main challenge associated with PD is that it is not feasible to it diagnosed until obvious symptoms are present in a patient, due to which several researches are going on to find

biomarkers which can help in finding early symptoms. Use and development of animal models has been increased for the past decade to understand the pathophysiology of PD, to determine why selective neurons die producing dopamine and finding out clues on how the PD develops. Gene therapy, stem cells, optogenetics, and advanced brain stimulating therapies are the few areas where researches are progressing on for the treatment of PD.

1.2 Methods available for the treatment of neurological disorders

There are several methods available for the treatment of neurological disorders and among those the treatments related to TMS are discussed here. The foremost method to treat any neurological disorder is through medication. All the other techniques of treatment for the neurological disorder are considered when medications have failed to produce any positive effect on the patient. For example, for treating depression, medications such as Serotonin reuptake inhibitor, antipsychotic and anxiolytic are given. Medical procedure such as electroconvulsive therapy is recommended only after the medications are failed.

1.2.1 Electroconvulsive therapy

Electroconvulsive therapy (ECT) has been used for more than 85 years for the treatment of psychiatric disorders [6]. It is administered by placing the electrodes on a patient's head, through which the electric current is passed into the patient's brain. Electrodes are placed either both sides (bifrontal, bilateral) or one side (unilateral) of the patient's head. The electrical stimulus is a bi-directional rectangular pulse with the width of one millisecond or more. The standard procedure of measuring ECT dose is in terms of the total charge delivered (millicoulombs).

Seizure is induced while the patient has been anesthetized and the brain activity is monitored by EEG (electroencephalography). ‘Seizure threshold’ is the minimum electrical dose required to induce seizure and this threshold varies from person to person based upon factors such as age, gender, skull density, medication and machine characteristics. Just after the anesthesia, muscle relaxation agent is administrated to reduce the possibility of injuries.

For major depressive disorders, ECT is preferred for the treatment of the extreme/urgent condition of patients who are involved in the suicidal attempts, plans or ideas for suicides, food refusal and hallucinations [7].

In the United States, ECT has been usually administrated three times per week, for total treatments of 6-12 times approximately, which is specific to different patients. It is administrated for both in- and out-patients [7].

One of the most common and adverse effects of ECT is the retrograde amnesia. Soon after the ECT, patients suffer from the loss of memory of the events which occurred before the treatment. This loss of memory can exist up to years. There are also other risks due to ECT such as Brain edema or Herniation for patients with risk of intracranial pressure, which are still a topic of debate among clinicians [8]. Other side effects of this treatment are headache, back pain, vomiting, nausea, and myalgia.

1.2.2 Transcranial direct current stimulation

Transcranial direct current stimulation (tDCS) is the technique in which electrodes are placed on the head and direct current in the order of few milliamperes (1-2mA), is passed through the cortex [9]. This current can increase or reduce neural activity based on the position and type of connection of electrodes as anodal stimulation causes excitation and cathodal

stimulation causes inhibition. The device for tDCS is battery operated and provide constant current in milliamps. The after effects of tDCS can be controlled through the current intensity and duration of stimulation. It was developed initially for the treatment of major depressive disorder as the effect of tDCS is induced through the modification of membrane depolarization. But this treatment technique does not seem to be helpful in other disorders such as Parkinson's disease, schizophrenia, Alzheimer's disease, and stroke.

1.2.3 Deep brain stimulation

Deep brain stimulation (DBS) is an invasive procedure involving surgery and implantation of electrodes into deep brain regions targeting specific structures within basal ganglia. These electrodes are used to send controlled weak electrical pulses to the specific targets in the brain to control tremors and dystonia [9]. A battery powered pulse generator is implanted in the chest which controls the stimulation frequency and intensity. DBS is FDA approved for the treatment of Parkinson's disease and essential tremors since 1997, dystonia since 2003 and Obsessive-Compulsive Disorder (OCD) since 2009. Despite the popularity of DBS, the exact mechanism of action is unknown, but one of the hypotheses is synaptic inhibition in neurons, in which the nearby neurons are inhibited by the electrical pulses through the electrodes.

Currently DBS is used for more than 100,000 patients and yet it has several side effects such as cognitive problem, numbness, speech problems, and other side effects such as strokes, seizures, infection and confusion [5]. In addition, the potential risks involving an invasive brain surgery also poses a risk for patients [5].

1.2.4 Vagus nerve stimulation [10]

The Vagus nerve is the part of the automatic nervous system (nervous system which is responsible for control of those bodily functions which are not consciously directed, such as breathing and heartbeat), where it starts from the brainstem and ends in the abdominal cavity passing through the neck, chest and abdomen. Vagus nerve stimulation (VNS) is a technique to stimulate the Vagus nerve through electrical or manual stimulation. VNS has been studied for the past couple of decades to understand its effect on automatic nervous system and it was FDA approved for the treatment of epilepsy in 1997 and later it was approved for treating chronic Treatment Resistant Depression (chronic TRD) since 2005.

All these treatment techniques discussed above uses some form of electrical stimulation, which comes with several discomfort and side effects for the patients going through these procedures such as from the pain caused during and after the treatment, side effects and the general fear of patients from being exposed to electrical shocks in their brain. The TMS technique discussed in the next section, should be a better alternative for patients, by solving most of the side effects that come with the other methods of treatment.

1.3 History of bioelectricity and TMS

Biological effects of electricity were first discovered by Italian physicist and physician Luigi Galvani in 1771 giving the birth of the field of electrophysiology. He used two different conductors to twitch the legs of a dead frog and concluded that muscles and electricity has some relation. Subsequently, bioelectricity was promoted in Europe by the Galvani's nephew Giovanni Aldini, who claimed that bioelectricity has the potential to revive the dead tissues [11]. He proved his theory by showing muscle contractions in the dead bodies of both animals

and humans when direct electrical current was passed through them. This encouraged the other scientists to perform gruesome experiments and perhaps to even cross the ethical limits of science. They did not respect the dignity of their test subjects or questioned their methods, while performing experiments. One of the example of such experiments was conducted by the American scientist Robert Bartholow, who applied electric current to a lady named Mary Raffery and continued to increase the current till Mary suffered from convulsion and went into coma. She died after 72 hours. This experiment clearly shows the importance of ethical guidance in medical science, since scientists can become blinded from the consequences to their experimental subjects, in the quest for knowledge. Today, there are rules and regulation to protect the test subjects including both human and animals and keep the experiments within ethical limits. Institutional Review Boards (IRB) makes sure that scientist, investigators and experimentalist gets proper training before performing experiments on humans or animals. Before conducting any new investigation, approval must be received from IRB, where the experimental methods must be described in detail, including the names of all the people involved in it.

Despite the ethical issues, continued experiments and application of electrical current to human subjects, in the eighteenth century, lead to the development of Electro-Convulsive Therapy (ECT) in 1937, by Italian physicians Cerletti and Bini. This was the beginning of the modern brain stimulation in the medical world. ECT was initially intended to treat the patients suffering from schizophrenia, but it quickly gained popularity among the psychiatrists to treat other brain disorders. This popularity lead to the overuse of ECT for various psychiatric disorders, causing serious side effects to the patients. There was a general repulsion for ECT among the public due to the side effects, leading to the existence of a stigma among the society

against therapeutic techniques like ECT. These practices made FDA regulate all the brain stimulation devices in 1976. Since then FDA oversees all the novel therapy techniques and ensures that they are regulated while developing and implementing and prevented any misuse by the practitioner.

The closet experiment to current TMS stimulator was performed in 1910, by Silvanus P Thompson who stimulated the head with magnetic field and saw flickering of light irrespective of whether eyes are open or closed (Fig. 1-1)[12]. In late 1970s, use of transcranial electric stimulation began to measure motor conduction time in the patients of sclerosis. This process caused extreme discomfort to the patients whereas TMS was the solution to it by providing similar motor conduction time with less discomfort and pain. Eventually over time, practitioners were largely interested in TMS as a diagnostics and investigational method, because of which, there were not much animal testing done with TMS, in order to explore the potential of TMS as a therapeutic technique on humans.

The physics behind TMS was developed by the English scientist Micheal Faraday in 1831, who observed that the alternating current can generate time varying magnetic field. In TMS, stimulating coils carry the alternating current to generate a time varying magnetic field on the order of few Tesla. This magnetic field induces electric fields in the brain which depolarizes the neurons at the site of stimulation. Unlike ECT, the only side effect of TMS was a slight risk of seizure in some patients.

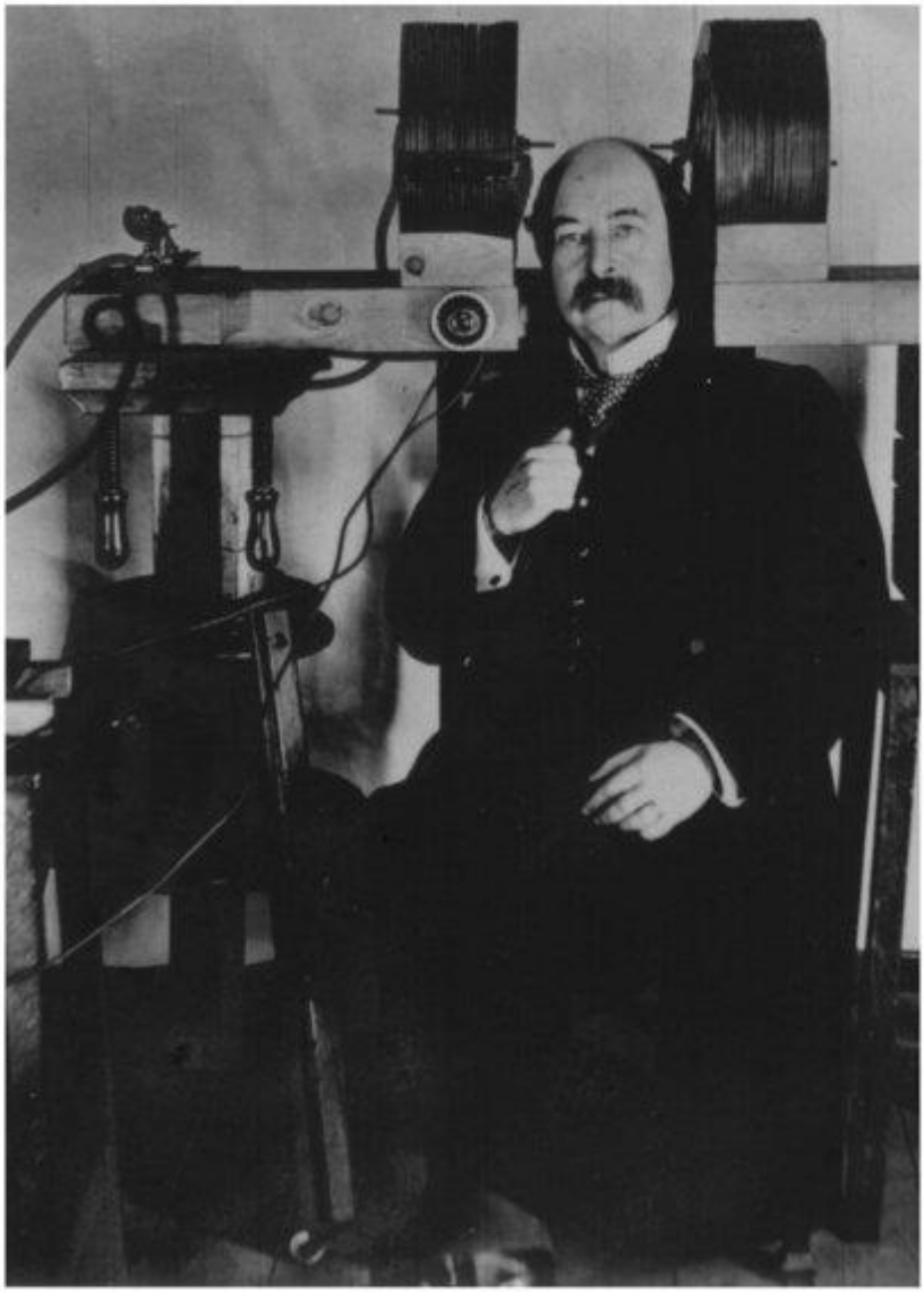

Figure 1-1. Silvanus P Thompson with his magnetic stimulator in 1910. (Transcranial Magnetic Stimulation, Scholarpedia)

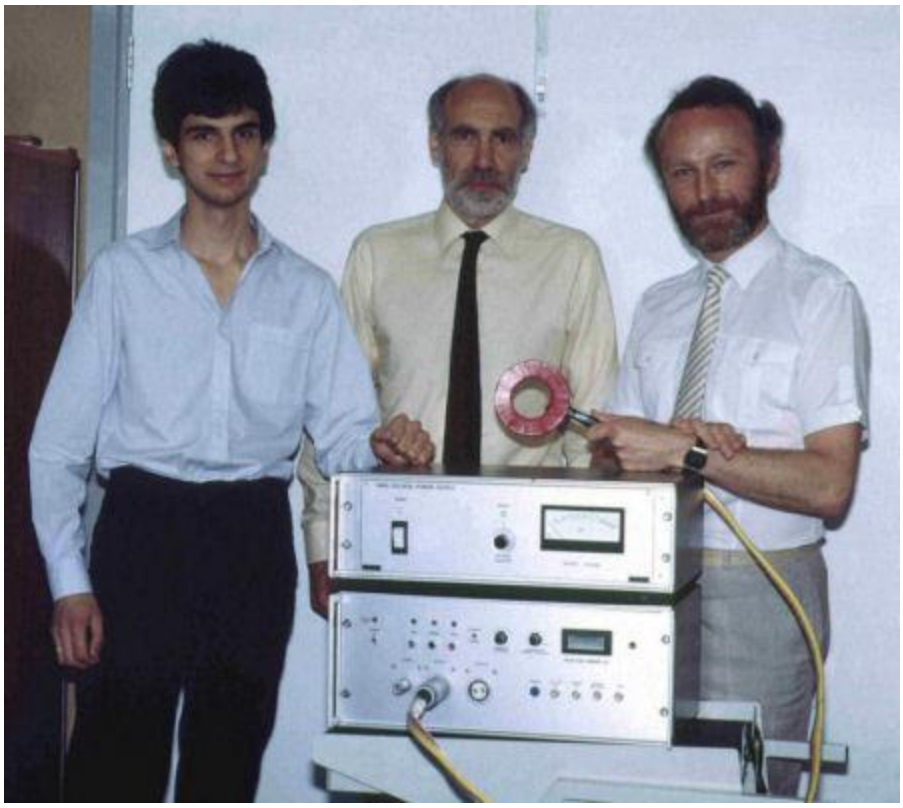

Figure 1-2. First proper working model of TMS stimulator in 1985.From left to right: Reza Jalinous, Ian Freeston and Tony Barker (Transcranial Magnetic Stimulation, Scholarpedia).

The first proper working model of TMS stimulator was developed by Anthony Barker and his colleagues in 1985 (Fig. 1-2). Since then TMS has undergone several stages of development and has been gaining popularity for the treatment of depression. Pascual-Leone *et al* at Howard expanded TMS from single pulsed to repetitive TMS (rTMS) in early 90s by reporting that rTMS can have lasting effects after stimulation session and it can be used as a therapeutic device [13], [14]. In 1988, Ueno et al developed a novel stimulating coil, namely the "Figure-of-8 coil" which was so popular due to its focality that it is still in use and FDA approved for the treatment of depression [15]. The very first clinical trial using rTMS was published by Kolbinger et al, where 15 patients suffering from Treatment resistant depression were studied and significant difference was found from the controlled group [16]. Furthermore, in 1996, a

group of leading experts and scientists in TMS met first time and decided the detailed safety guidelines for TMS in both clinics and research labs.

In 2007, Neuronetics Inc, received FDA approval for the treatment of specific forms of medication- refractory depression (FDA approval K061053). Soon after in 2008, NeuroStar obtained FDA approval for TMS therapy for specific population who have failed to response to not more than one antidepressant medications. These were the initial FDA approval related to TMS and since then TMS has made significant progress in terms of treatment and therapeutic benefits. In the next section, the mechanism behind TMS will be discussed from both physics and biological point of view.

1.4 Mechanism behind Transcranial Magnetic Stimulation

TMS is based on the Faraday's law, where electromotive force (emf) generated around a closed conducting path is equal to the negative of time derivative of the magnetic flux density passing through the closed loop. This time varying magnetic field determines the induced electric field on a conductor present in the vicinity of the primary current carrying conductor. Differential form of Faraday's law is shown by equation 1.

$$\nabla \times E = -\frac{\partial B}{\partial t} \tag{1}$$

In TMS, a pulse is generated which rises steadily and falls sharply back to zero, with a pulse duration of less than 1 ms. This change in the electric pulse generates a time varying magnetic field which is perpendicular to the current carrying coil with the magnitude of 1-2 Tesla. This varying magnetic field penetrates inside the patient's head, decaying at the rate of inversely proportional to the cube of distance and induces electric field in the brain. This

generates eddy current parallel to the TMS coil, but with the current direction opposite to the one in the TMS coil. This induced electric field is shown by the integral form of Ampere's law in equation 2.

$$\oint E \cdot dL = -\iint_S \frac{\partial B}{\partial t} \cdot dS \tag{2}$$

The eddy current inside the brain depolarizes the neurons through action potential, but the exact mechanism of how the TMS works is still unknown. This unknown factor could be contributing to the variation in the effectiveness of TMS across different subjects.

Despite this unknown factor, it is still worthwhile to try to understand the basic structure of nervous system, in order to comprehend the ways that TMS could affect a patient. The nervous system is made of neurons and glia cells, where neurons are responsible for receiving and transmitting electrical and chemical signals and glia cells plays a role in supporting neurons. Neuron structure can be broadly divided into three parts: dendrites, synapses and axons. Dendrites are the branched projection which are tree-like structures, that are away from the cell body and used to receive information from the other neurons through synapses. Synapses are the end points of the neurons which are used to exchange the information with another neuron. Axons are long, slender tube-like structures that send the information to the other neurons, muscles and organs. Neurons can be classified into four major types, unipolar, bipolar, pseudounipolar and multipolar, whereas there are seven types of glia.

Human nervous system is very complicated, comprising around 100 billion neurons which form trillions of connections throughout. Furthermore, the nervous system has two main parts: the central nervous system (CNS) and the peripheral nervous system (PNS). CNS consists of

brain and spinal cord and PNS includes nerves which connects CNS to the different parts of the brain.

In TMS, an induced electric field is required to provide the minimum required potential difference for the action potential and cause successful firing of the neurons. Action potential plays a significance role in the cell to cell communication in neurons. Most of the cell membranes maintains a voltage difference between the inside and outside of the cell, which is called the membrane potential. Typically, the voltage inside the cell is -70 mV which is also called the resting potential and it is at the relatively negative voltage than the cell exterior voltage. When there is an electrical signal, the membrane potential rises to -55 mV, called the threshold potential. Action potential occurs when the voltage rises upward to +40 mV and falls back rapidly to the same level within few milliseconds as shown in Fig. 1-3. Furthermore, sodium ions level increases as the membrane potential increases, which is followed by the exit of potassium ions from the cell. Depolarization occurs when the concentration of the sodium ion increases in the cell, and the potential of the cell is higher than its resting potential. As the process continues, influx of the sodium ions stops at the peak of the action potential, whereas potassium ions continue to exit the cell, which causes the cell to hyperpolarize. Hyperpolarization is opposite of depolarization where the cell's membrane potential is negative and it inhibits the action potential by increasing the required threshold value for the action potential.

To get the required action potential, TMS stimulators need to be designed carefully to provide the correct duration and intensity of electrical stimulus. In the next section, design of the TMS stimulator is discussed briefly.

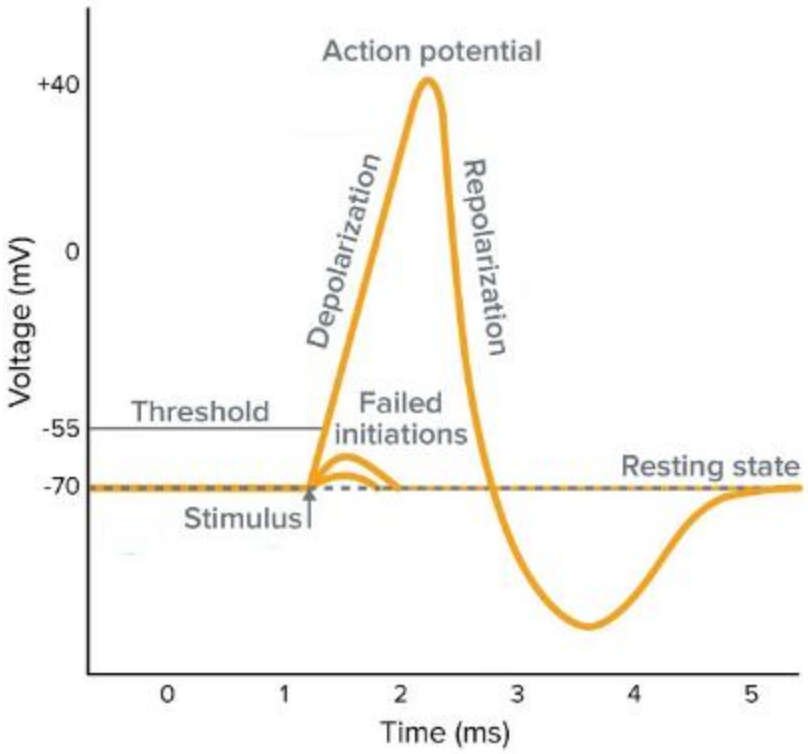

Figure 1-3. The various phases of action potential (action potential, Wikipedia).

1.5 TMS Stimulator

TMS stimulator are the generators of time varying magnetic field in the TMS coils. A large current (~5000A) is required to generate the magnetic field of the order of 1-2 Tesla. A capacitor or a capacitor bank is used to charge and discharge the TMS coil for each pulse. The basic working principal of the TMS stimulator can be explained with the stimulator system being divided into three main blocks, namely, the AC to DC conversion block, capacitor charging block and discharge cycle block (Figure 1.4). In the first block, 120 VAC power supply is converted to DC with the help of capacitors and diodes. In the second block, the converted DC voltage is stepped down to the required voltage level with the help of resistors

and potentiometers, and it is used to charge a capacitor (C3). This capacitor plays an import role in the stimulator as it needs to be charged and discharged for every pulse while operating in rTMS mode. Mostly there is a user control switch present in the TMS stimulator, which can be operated by the user to charge or discharge the capacitor manually. Once the capacitor is charged, it discharges into the TMS coil which is represented by the inductor L1 in the Fig.1-4. A switching device (SCR, IGBT or BJT) is used to control the pulse width along with the rise and fall time of the electrical pulse. A pulse is typically 400μs in width with a rise time of 100μs. Furthermore, the TMS coil is made of thick insulated copper wire which can carry a large of current. The wire can be either round or rectangular in shape.

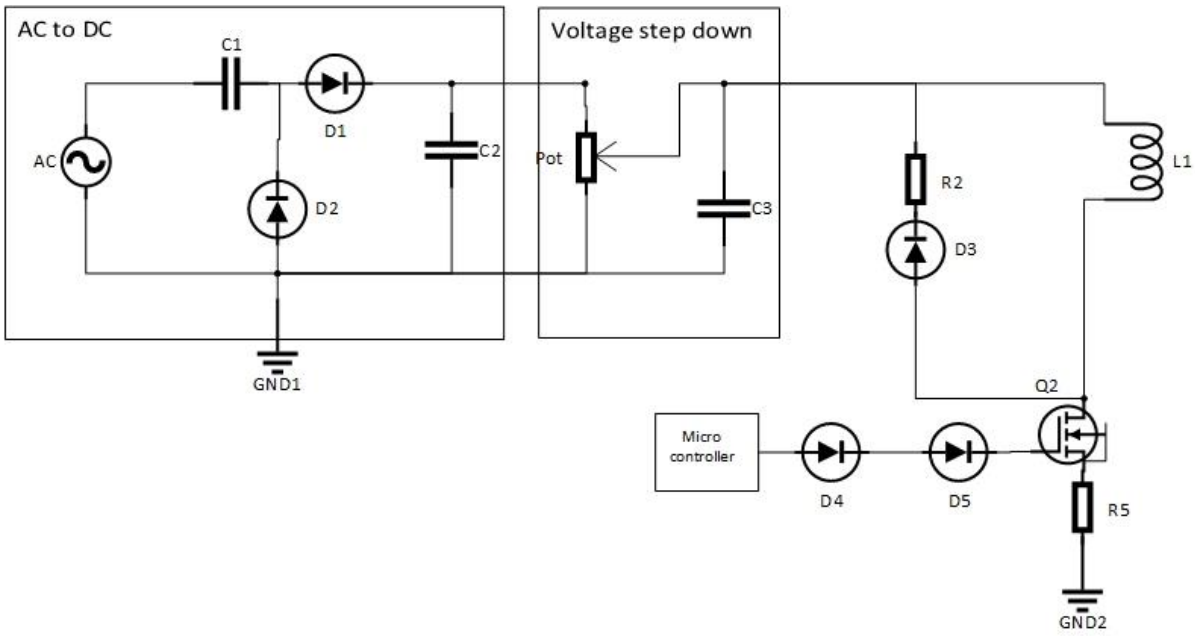

Figure 1-4. The TMS stimulator with basic components, which are divided into three blocks (Selvaraj et al [17]).

The TMS stimulator unit can be one of two types: monophasic and biphasic. A monophasic stimulator generates the voltage only in one direction. Since, the voltage is unidirectional, the magnetic field also induces the electric field in one direction with every pulse. Initially, TMS stimulators were developed as monophasic. Such monophasic stimulators are still in use, due to their circuit simplicity. Furthermore, they are useful, when unidirectional magnetic field is essential specially for research purpose. Biphasic, also known as polyphasic stimulators, can generate pulses with voltages in both the positive and negative direction. Hence, the magnetic field is also produced in both positive and negative direction. So, for every pulse, there is one positive and one negative pulse. Biphasic stimulators are more popular than the monophasic counterparts and are used for the treatment of depression.

There are several manufactures of TMS stimulators and coils in the market, which makes devices for both commercial and research purposes. Those discussed in the next section are the main players in the TMS market and have FDA approval for their stimulator systems.

1.6 TMS in commercial aspect

A research team (Mike Polsan, Anthony Barker and Ian Freeston) at Sheffield University, UK in 1982 successfully proved TMS as a testing method for brain. Novametrix Medical System Inc. took this work commercially. Later, this company was named Magstim, which continues to be the leading manufacturer for TMS coils and equipment. Currently, they manufacture variety of TMS coils including air cooled coils, liquid cooled coils, and monophasic/biphasic TMS stimulators [18].

Neuroneutics, a US based company have a product called Neurostar TMS therapy system, got FDA approval for their TMS device in 2008, for the treatment of major depressive disorder. In 2009, they also worked to get the first insurance coverage for the TMS treatment [19].

Magventure is another company which manufactures coils and stimulators, started their first TMS stimulator in 1992 and the stimulators were sold under the brand name Dantec. This company was established with the name of Magventure since 2007 and have done pioneering work in static and dynamic cooling concepts, which allowed researchers to perform rTMS sessions without changing the coil. They received FDA approval for the treatment of depression in 2015 [20].

Brainsway is the manufacturer of the Hesed coil, which is also FDA approved for the treatment of depression. They also claim that their coil can stimulate deep brain regions. Hesed coil is a complicated coil which covers the entire head like a helmet and stimulate relatively large area when compared to the Figure-of-8-coil.

All these devices mentioned above are FDA approved for the treatment of depression or for the region related to the cortex of the brain. From this summary of commercially available TMS products, it should be clear that coil design is very important in order to use TMS for treating other neurological disorders or to stimulate different regions of the brain.

1.7 Importance of coil development and head modelling

TMS has come a long way in the past 30 years since its invention in 1985 by Barker et al. It's also gaining popularity for the treatment of major depressive disorder. TMS coils can navigate the magnetic field to the required region with the help of different coil geometries.

The first coil which was used with the TMS stimulator in 1985 was the single circular coil. This coil was in a circular shape as its name suggests, with all the turns in a single plane. This was the simplest coil, yet it never gained approval from the FDA, since this coil never showed any advantage when compared to Figure-of-8 coil. The Figure-of-8 coil was developed in 1988 by Ueno, followed by the development of TMS stimulator in 1985 [15]. This coil gained immediate popularity due to its small spread of magnetic field, and similar amount of induced electric field when compared with the circular coil. Figure-of-8 coil has two sets of circular coils which are placed adjacent to each other, with the currents flowing in the opposite direction. This directional current flow ensures that the induced electric field adds up at the center of the coil. There are several variations of the simple Figure-of-8 coil developed over the years, such as changing the number of turns, varying the size of the coils, giving an angle in-between the coils, or placing another set of Figure-of-8 coil on top of the first one. One of the example of such change is by the manufacturer Neuronetics, who added an iron core to the Figure-8-coil.

The Hesed coil, developed by the Brainsway has a complicated geometry. It has the shape of a helmet along with a tiara, which is placed close to the forehead. It is also FDA approved for the treatment of depression. Brainsway claims that their coil is suitable for the deep brain stimulation [21]. There are several generations of this coil developed over the years, which are protected by the intellectual property rights.

Crowther et al developed the “Halo Coil” which was placed 100 mm below the head [22] and it was intended to use with either circular or Figure-of-8 coil as the top coil. The Halo Coil improved the magnetic field strength by 50% at 50 mm in comparison to circular coil and has the potential to be used for several deep brain disorders treatment.

Furthermore, finite element tools are essential in order to calculate the magnetic and induced electric field, as hand calculation of these parameters will be extremely difficult due to the complicated shape of the coils. Calculation of accurate value of the induced electric field depends on the accuracy of the head model, as induced electric field is affected by the permittivity and conductivity of the brain tissues and segmentation. Hence computer modelling speeds up the research time and reduces the cost of the development when compared with clinical trials.

A couple of years ago, homogeneous head models or spheres were used for the calculation of magnetic and induced electric field. In these models, calculation of magnetic field was correct but electric field was inaccurate due to the same value of conductivity and permittivity used for the entire head model. Currently, there are various commercial human and animal models available with increased segmentation and high resolution such as Duke, Ella, Mida [23].

In the present work, development of two TMS coils for humans with one focusing on the deep brain stimulation and other on the precision of stimulation have been discussed, which will be followed by the development of 50 MRI derived heterogeneous head model development and comparison of different animal coils.

CHAPTER 2

DEVELOPMENT OF A NOVEL DEEP BRAIN COIL - TRIPLE HALO COIL

This chapter has used materials that were published in the paper "Transcranial Magnetic Stimulation: Development of a Novel Deep-Brain Triple Halo Coil", by P. Rastogi et. al, with the permission of all the authors [46].

Transcranial Magnetic Stimulation (TMS) was introduced by Barker over 25 years ago as a neurophysiological technique for non-invasive stimulation of the cortex [24]. Since then, there was extensive development in TMS research with the invention of various coil designs and stimulation techniques [25]–[36]. Now there are many different coil designs that have been developed which vary both in depth of stimulation and focality. These have been reviewed by Deng *et al.* [37] and Guadagnin *et al*.[37]–[39].

A significant limitation of all TMS coils, is that the direct stimulation they provide is largely restricted to superficial cortical targets. Researchers have worked to overcome these limitations, and arguably two most of the most notable advances have been the Hesed Coil (H Coil) by Zangen et. al [40] and the Halo Coil by Crowther et. al [41]. All coils aimed at deep brain stimulation suffer from the known trade-off between stimulation focality and depth [39]. The H-Coil aims to increase the depth of stimulation, while still maintaining moderate focality, and has been shown to be useful in several studies [42]. Alternatively, the Halo Coil can stimulate a much larger volume of the brain without regard for focality, in order to increase as much as possible the stimulation received by deep brain structures [43].

Among the FDA approved TMS coils for major depression, the H-coil stimulates the lateral frontal regions to a depth of 6 cm from the surface of scalp, which is deeper stimulation than

the Figure-8 coil. The measurements to determine the depth of stimulation were taken with the help of a homogeneous head model filled with physiologic saline solution [44].

This chapter presents a novel multi-coil configuration which induces higher E-field in comparison to the Halo Coil, with an effort to overcome the limitations of the same. Magnetic fields decay rapidly with the distance from their source (coil surface); therefore, it is challenging to develop TMS coils which has high magnitude of magnetic field at deep brain regions. Moreover, TMS coils that stimulate the deeper regions of the brain tend to over-stimulate the surface of the brain while trying to reach the deeper regions of the brain. To overcome these problems, the authors have proposed a novel coil configuration called the "Triple Halo Coil" (TH Coil) [45]. This coil configuration stimulates deeper regions of the brain with more than 7 times higher magnetic field at a depth of 10 cm for the same amount of surface field of a Figure-8 coil with same amount of current in each coil windings.

The geometry of coils plays an important role in the stimulation of the brain. TH Coil configuration uses elliptical coils to overcome the shortcoming of the Halo Coil, which has uniform magnetic field due to its circular shape around the head. It was found that the magnetic field in the deep brain regions such as the thalamus, hypothalamus, hippocampus, and mid brain generated by the TH Coil has increased many folds, when compared to the commercially available coils such as the Figure -8 coil. With the use of the TH Coil, deep brain regions, related to the neurological disorders such as Parkinson's disease, and PTSD can be stimulated non-invasively, which is not possible with commercially available coils without excessively stimulating non-targeted, superficial cortical regions [46].

2.1 Method

The magnetic field generated by the coils and induced E-field in the brain was calculated on a heterogeneous head model using a finite element analysis tool: SEMCAD X and Sim4life [47][48]. Iterative modeling aided in the development of novel coils by testing the distribution of electric and magnetic field in the brain. A quasi-static model has been used for the calculations and the vector potential can be calculated by the Biot-Savart law as shown in equation (2-1).

$$\vec{A}_o(\vec{r}) = \frac{\mu_o}{4\pi} \int_{\Omega} \frac{\vec{J}_o(\vec{r}\,')}{|\vec{r} - \vec{r}\,'|} d\vec{r}\,' \qquad (2\text{-}1)$$

The vector potential **A** is decoupled from the electric field **E**, which is calculated by equation (2-2)

$$\vec{E} = -j\omega\vec{A} + \nabla\varphi = \vec{E}_s + \vec{E}_i \qquad (2\text{-}2)$$

The anatomically realistic heterogeneous head model used for the current study was developed by IT'IS Foundation [23], [49], [50]. This model was generated from MRI data of a 34-year-old male adult and consisted of 44 different tissues. These tissues were assigned their corresponding electric conductivity, and magnetic permeability at the operational frequency of 2500 Hz. The peak current in the coils was 5000 A (100% power level) in the simulations, which was same in all the comparison coils. The reason for keeping the current to 5000 A is because it is the maximum current which can be supplied with a Magstim power supply. The TH Coil used only 70% of the total power while testing as explained in the results section.

The TH Coil configuration consists of three large coils placed around the head as shown in three different colors- red, blue and green in Figure 2-1. These large coils of the TH Coil are

elliptical in shape, instead of spherical as in the Halo coil in order to reduce the stimulation on the face and have a sufficient amount of stimulation in the deeper parts of the brain. The distance between the anterior portion of the TH Coil and the face can be adjusted due to the large size of the coils. The eccentricity of the elliptical coils in the TH Coil is 0.74, which has been chosen after several iterations based on the E-field profile in the heterogeneous head model.

There was a tradeoff between over stimulation on the outer surface of the head model and high stimulation in the deeper regions of the head. Hence, coil shape and size was finalized taking both into account and choosing between over stimulation of peripheral areas and over stimulating subcortical structures. All the three toroids have four windings in the TH Coil configuration, with the inner toroid having 0° angles, middle toroid having 30° angles, and the outer toroid having -30° angle with respect to axial plane. Similar to the coil geometry, the angles between each portion of the coil was optimized to maximize the subcortical stimulation while reducing stimulation to peripheral regions. The inner radii of the elliptical coils are 200 mm and 300 mm. The vertical center of the TH Coil is 110 mm below the vertex of the head.

The induced E-field from the TH Coil alone and in conjunction with the Figure-of-8 coil was studied and comparison was conducted along the coronal and sagittal planes. The axial plane of the E-field at 2 cm interval up to 10 cm from the top of the head was taken to illustrate the simulated regions of the brain. Decay rates of the magnetic field from various coils such as the circular coil, Figure-of-8 coil, and Halo coil have been compared with the TH Coil alone and TH Coil- Figure-of-8 coil combination.

2.2 Computer modelling and experimental results

2.2.1 Finite Element Analysis

The induced E-field from the TH Coil alone and TH Coil with Figure-of-8 coil has been in illustrated in Fig. 2-2. In both instances, the induced E-field was increased in the deeper regions of the head when compared to the stimulated regions due to the Figure-of-8 coil operated alone. TH Coil, has induced higher E-field in both the deep and outer edge of the head model i.e. in the posterior portion of the model than in anterior regions due to its asymmetrical positioning around the head model.

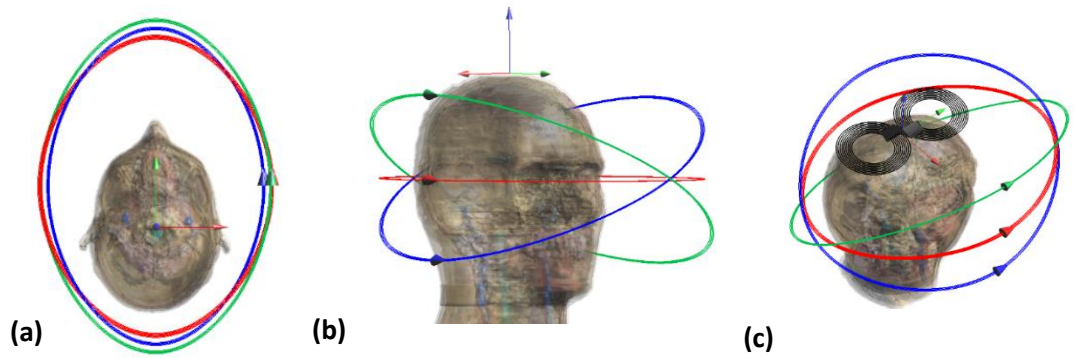

Figure 2-1. The TH Coil configuration with and without Figure-of-8 coil on the heterogeneous head model. The three colors of the TH Coil represent the three coils in the elliptical shape. Red color represents the inner toroid, blue color- middle toroid and green color- outer toroid. The black color coils illustrate the 70 mm Figure-of-8 coil.

The Figure-of-8 coil was used along with the TH Coil to stimulate the cortex, since TH Coil does not stimulate the top of the head. Stimulation of deeper brain regions is due to the TH Coil alone which can be seen in Fig. 2-2 (b) and (d). It can also be seen that in the sagittal plane the TH Coil stimulates a large portion of the brain including deep regions of the brain (Fig 2-2).

The current in the Figure-of-8 coil flows in such a way that there is a summation of the current at the center of the coil. The Figure-of-8 coil has current both in the same and opposite directions to the TH Coil, which leads to a net cancelation and summation of E-Field intensities in the model. Sagittal plane (Fig. 2-2b) of TH Coil with Figure-of-8 coil shows that there is a decrease in E-field on the facial region including eyes and surrounding area, whereas, sagittal plane with TH Coil alone (Fig. 2-2d) has a continuous stimulation on the frontal region of the head model.

Fig. 2-2(a) and (c) show the centered coronal plane of the E-field in the heterogenous head model. Position of the slice is also shown in the inset at the lower right corner of Fig. 2-2(a). The Figure-of-8 coil only stimulates the top 2 cm of the head which is not stimulated when TH Coil is used without Figure-of-8 (Fig. 2-2c). The rest of the stimulation in the lower part of the brain remains the same with and without the Figure-of-8 coil as discussed above.

There is almost zero field in the center of the brain but it has not stopped the stimulation in the regions such as hippocampus. The maximum E-field in the hippocampus is 99V/m which is close to the threshold limit of neural activation, given the 5000 A in each coil. Overall E-field is higher at the periphery of the brain and decreases towards the center of the brain. Olfactory regions of the heterogeneous head model have the highest stimulation due to the higher conductivity of that region. Elliptical shape of the coil was developed to increase the distance from the facial part of the head model and decrease the stimulation of the olfactory.

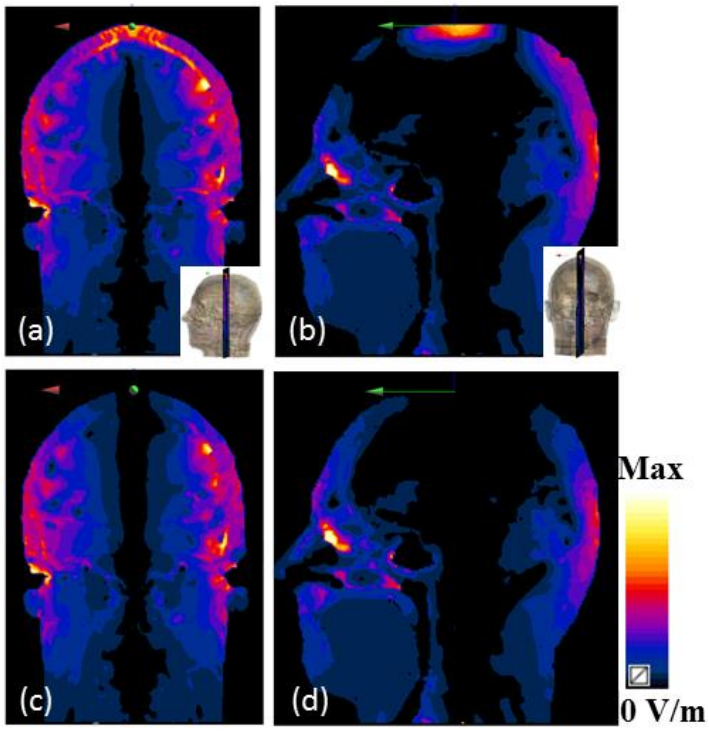

Figure 2-2. The E-field on the heterogeneous head model (a) Coronal view- TH Coil with Figure-of-8 coil (b) Sagittal View- TH Coil with Figure-of-8 coil (c) Coronal View- TH Coil without Figure-of-8 coil (d) Sagittal View- TH Coil without Figure-of-8 coil. Position of the slice in the heterogeneous head model are shown in the inset of (a) and (b). The E-max value is 350 V/m when 5000A of current slows in each coil.

The five axial planes (Fig. 2-3) give a complete profile of the E-field stimulation in the brain when stimulated with the TH Coil along with the Figure-of-8 coil. Fig. 2-3(a) shows that that the top of the head is stimulated with the highest overall field. The orientation for the Figure-of-8 coil was considered because it maximized the E-Field intensity. Due to the cancellation of the magnetic flux with the help of opposite current direction in the TH Coil and front coil of Figure-of-8 coil, the E-field is almost zero in the frontal lobe of the head model (Fig 2-3b). As the stimulation due to the Figure-of-8 coil becomes zero with increases in distance from the coil, the E-field (Fig. 2-3c) mainly stimulates the periphery of the slice.

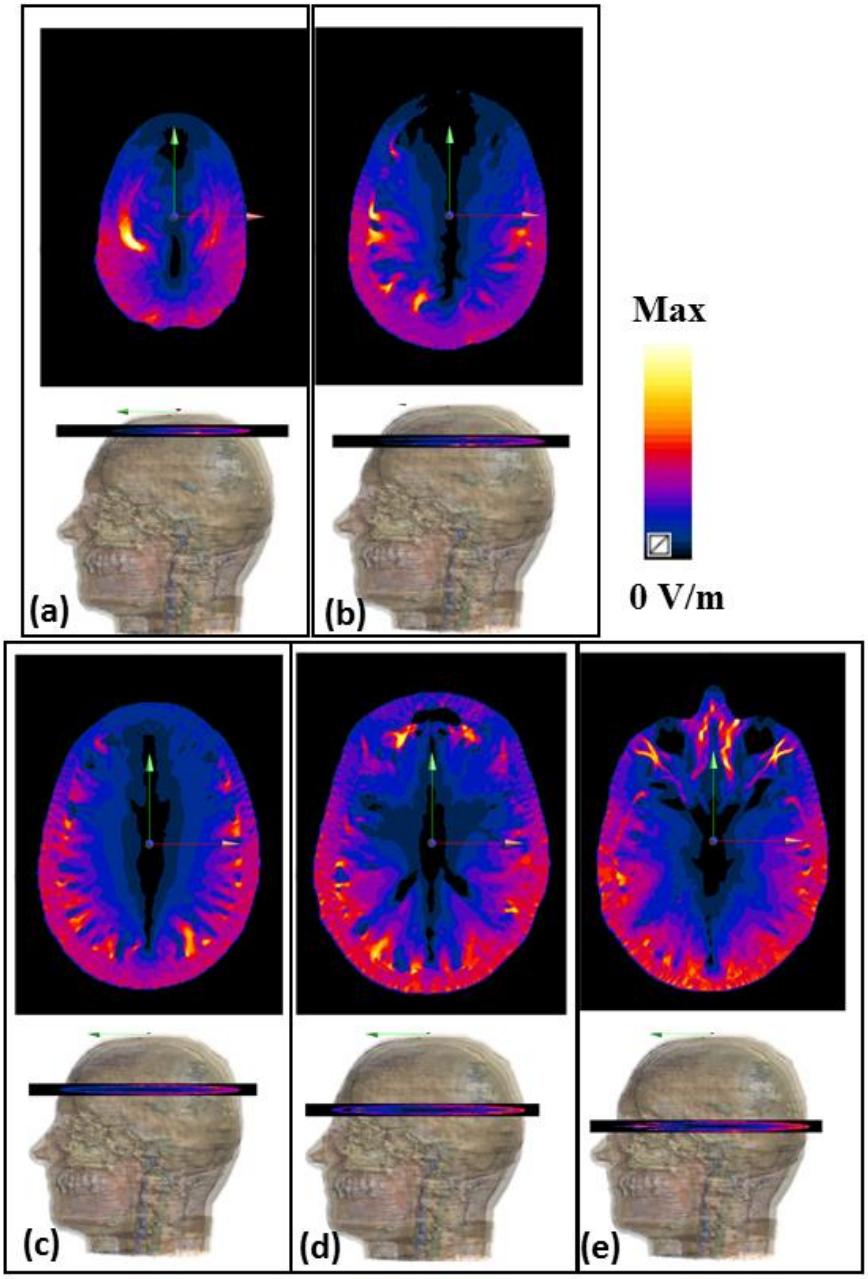

Figure 2-3. The E field in the heterogeneous head model induced by TH Coil and Figure-of-8 coil along the axial planes: (a) 2 cm (b) 4 cm (c) 6 cm (d) 8 cm (e) 10 cm from the top of the head. Position of the slice in the head is shown right below the E field of the slice. The E-max value is 350 V/m when 5000A of current slows in each coil.

The E-field simulation increases as in the slice at 8 cm (Fig. 2-3d) due to the cross section of the TH Coil. Axial slice (Fig. 2-3e) passes through the eye lens, sclera and vitreous humor.

The table 2-1 presents the 10^{th} greatest voxel (value) of the maximum E-field in the given region of the brain. This table shows that sensitive regions such as regions related to eyes are not stimulated with TH Coil while giving sufficient E-field in the required regions. All these values are given for the 5000 A of current flowing through the coils. The surface E-field in these and few more regions are shown in the Fig 2-4 where the maximum scale has 224 V/m.

Table 2-1. The maximum E-field value in important parts of the brain and related regions.

Parts	**E-field (V/m)**
Cerebellum	109
CSF	119
Eye Cornea	27
Eye Lense	21
Eye Sclera	46
Eye Viterous Humor	16
Gray Matter	190
Hippocampus	69
Hypothalamus	10
Mid Brain	41
Skin	209
Thalamus	22
White Matter	136

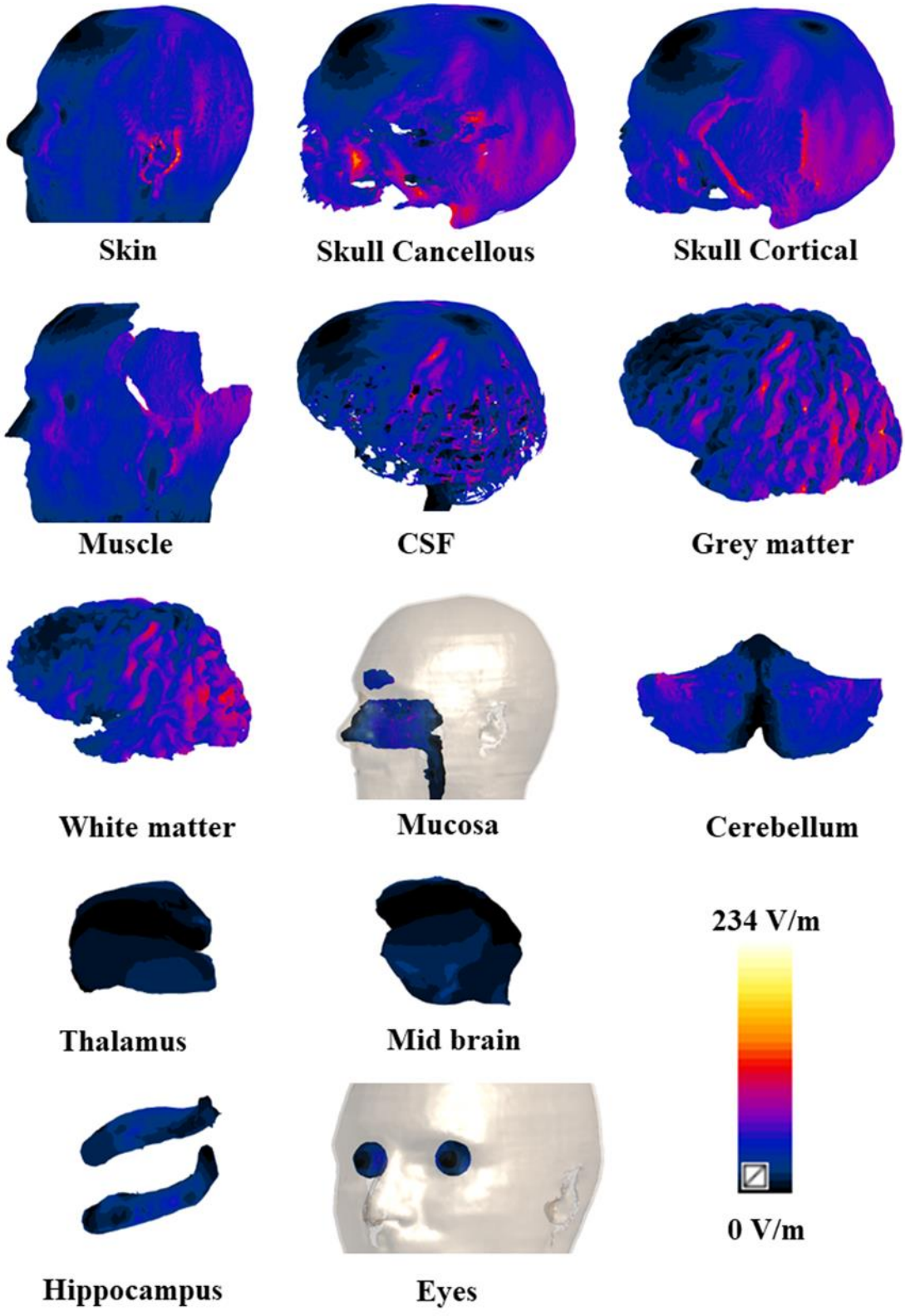

Figure 2-4. The surface E-field in different parts of the brain due to Triple Halo Coil and Figure-of-8 coil configuration.

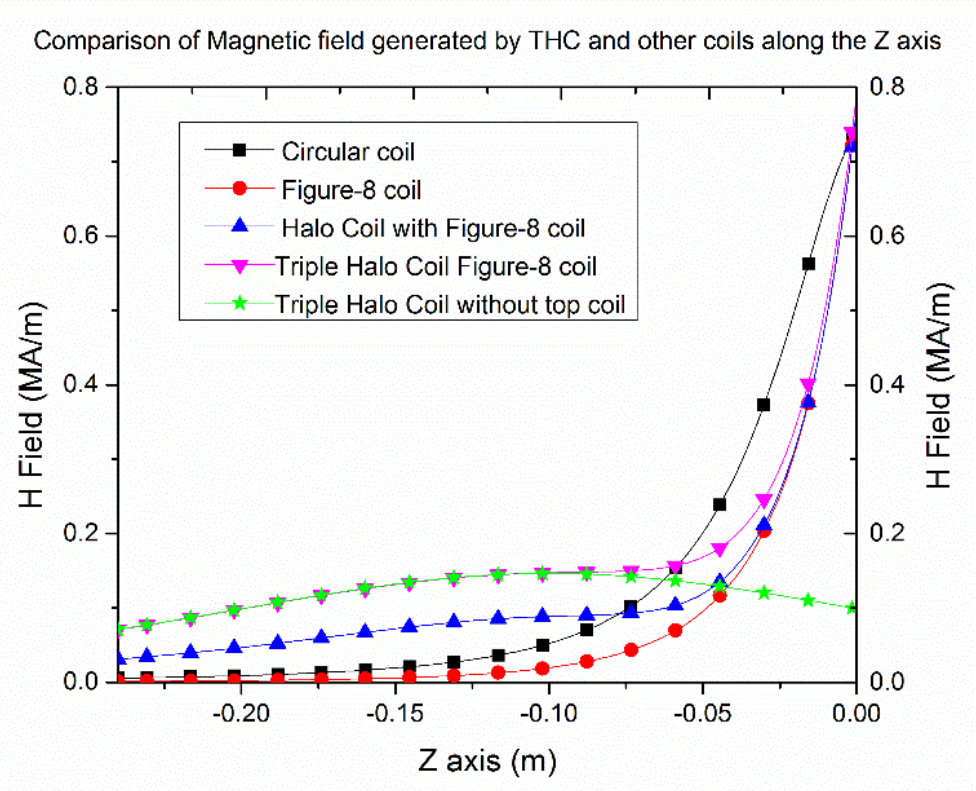

Figure 2-5. Comparison of magnetic field generated by TH Coil and other coils along the Z axis, through the vertex of the heterogeneous head model. Magnetic field at 10 cm below the surface of the head generated by the TH Coil in combination with Figure-of-8 is increased by more than 7 times when compared with the Figure-of-8 coil alone.

Fig. 2-5 illustrates the comparison of the magnetic field generated by different coils. Since the permeability of the human head is approximately 1, the magnetic field inside the head does not depend upon the different structures of the brain, which is different from E-field. All the coils for the comparison have the same current and their positions relative to the head model were kept constant. The decay rate of the magnetic field was taken at the vertex or the highest point of the brain, where there is an intersection of sagittal and coronal plane. The magnetic field due to TH Coil with the Figure-of-8 coil decreases at the same rate as the other coils, but after 5 cm below the vertex of the head, the value of magnetic field (H field) due to TH Coil is

133 kA/m without Figure-of-8 coil and 167 kA/m with the Figure-of-8 coil whereas the magnetic field is 199 kA/m due to circular coil, 94 kA/m due to the Figure-of-8 coil and 119 kA/m due to Halo Coil. The magnetic field at 10 cm below due to TH Coil with Figure-of-8 coil is 147 kA/m while 146 kA/m without Figure-of-8. Also, the magnetic field generated by the rest of the coils are: 51 kA/m due to circular coil, 19 kA/m due to Figure-of-8 Coil and 88 kA/m due to HC. Hence, the magnetic field generated by TH Coil is more than 7 times than the Figure-of-8 coil at 10 cm below the vertex of the head, and the difference increases as the distance increases. The green curve of the TH Coil in Fig. 2-5 confirms the existence of null E-field at the top of the head when it is not used in combination with any other coils.

2.2.2 Experimental verification

The prototype of the TH Coil configuration was fabricated with the help of Jali Medicals Inc. and it is compatible with the Magstim Stimulators [51]. Fig. 2-6 illustrates the prototype of the TH Coil configuration along with a commercial Figure-of-8 coil on a manikin head. The prototype dimensions are same as the computer model as mentioned in the finite element analysis modelling section.

Since, all the three windings are connected with one stimulator in parallel, the commercial stimulator was only capable of supplying 75% of the power to the coils for this prototype due to the low inductance of the windings. The windings were connected in parallel to reduce the overall induction of the coil system and did not distort the TMS pulse waveform as compared to connecting them in series. Accordingly, all the testing was done at 70% power level which corresponds to 3500 A of current from the stimulator.

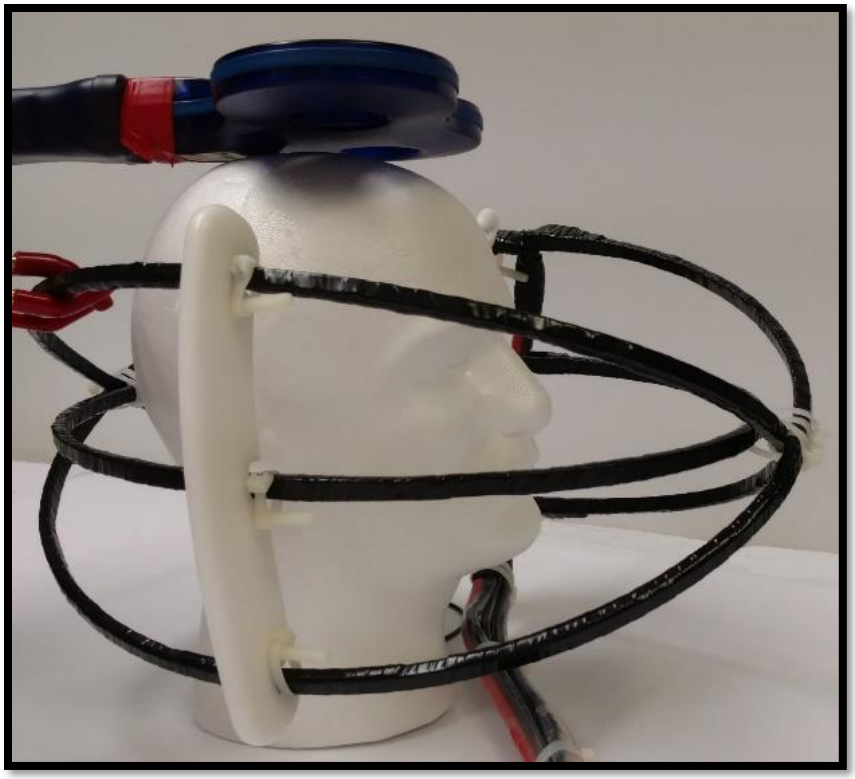

Figure 2-6. Triple Halo Coil configuration along with a commercial Figure-of-8 coil on a manikin head.

Hence, each of the three windings received approximately one third of the total 3500 A of current. Fig.2-7 illustrates the H field values out of the plane with respect to the inner coil (red color in the Fig.2-1) corresponding to 1167 A of current flowing through the coils in computer modelling and 70% of power in the prototype. It could be expected that there will be slight variation in the value of the current in each winding as the size of each winding is different leading to the difference in the total resistance. This is the limitation of this coil configuration while using a single stimulator. If these three coils are stimulated by three individual stimulators, then current in each coil winding can reach up to 5000A.

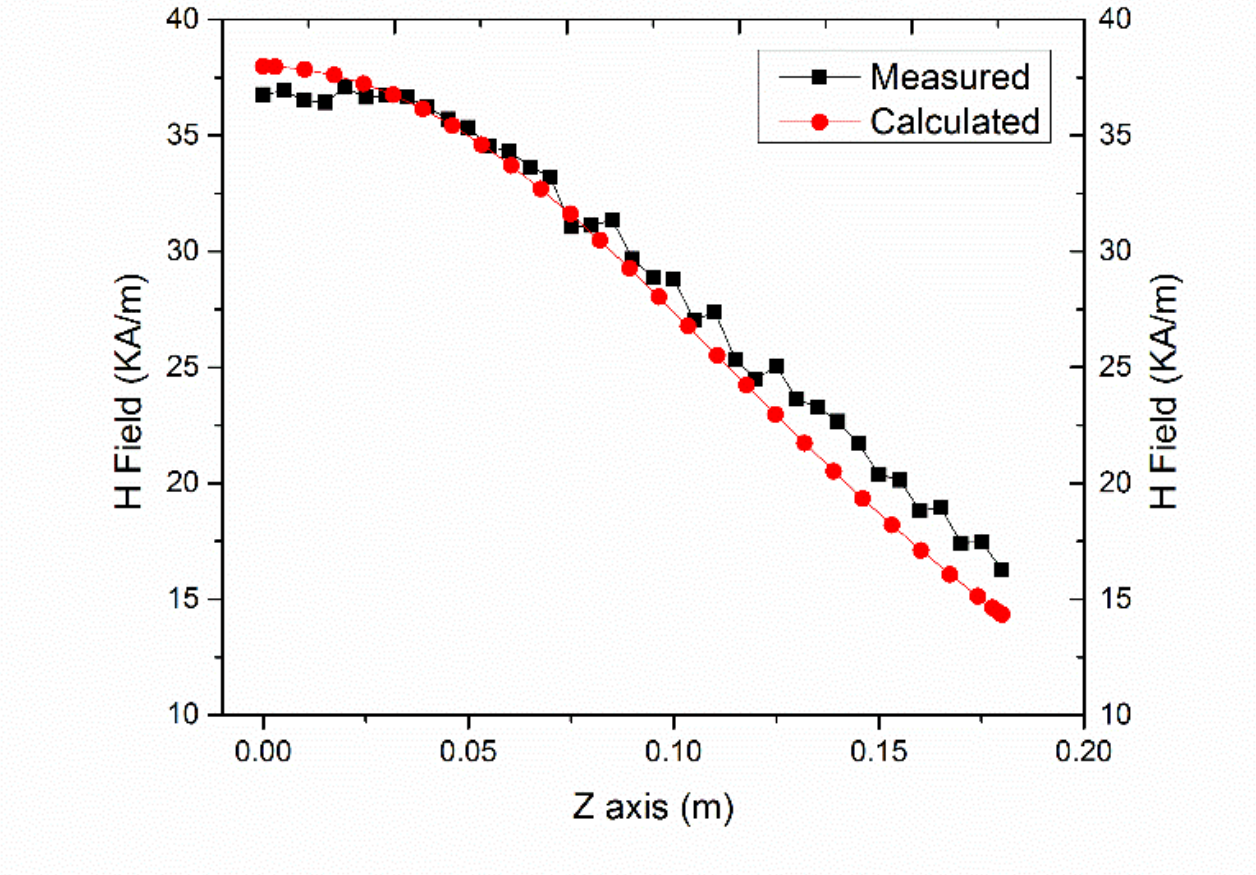

Figure 2-7. Comparison of magnetic field from the center of the coil and moving out of the plane with respect to the inner coil by FEM modelling and measurement.

Furthermore, there was an additional problem with this specific prototype. Fig.2-8(a) & (b) shows the "zoomed-in" image of the side of TH Coil windings. The cables are connected along the windings of the coils (12.4 cm) causing non-uniformity in the thickness (maximum 1.8 cm) of the windings. These extra connections have more current flow through them, thus contributing towards the increased H-field around the windings. In computer simulation, it is very difficult to model due to the non-uniformity of the connections but a simplified attempt was made using another finite element tool- Ansys Electromagnetic software, which is discussed in the next section. The above mention connection issue introduces small difference in the value of stimulation and measurement. However, this increase in H-field and non-

uniformity could be avoided through small modifications of design while manufacturing in future prototypes.

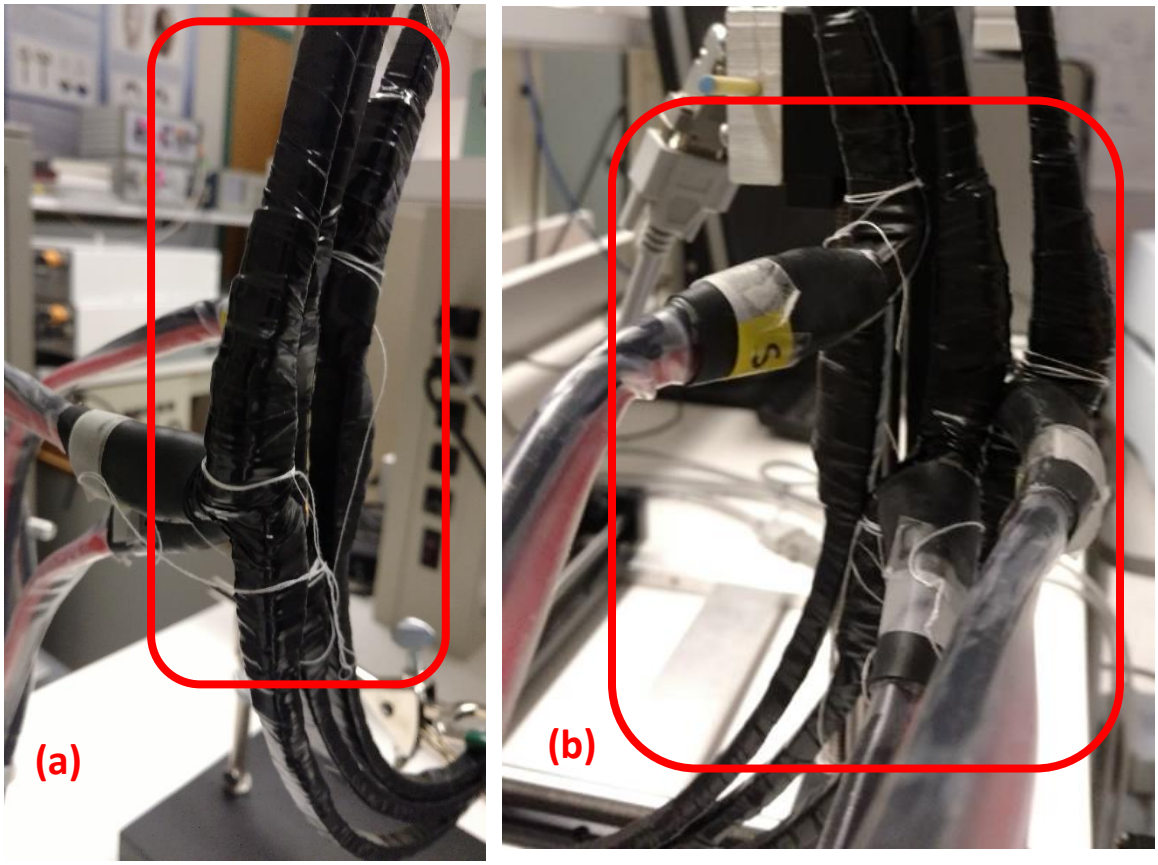

Figure 2-8. All the three windings were flattened to a plane for a clear view of the connections to the coils (a & b). The wires connecting the windings are 6.2 cm up and 6.2 cm down along the curve from the connection point and have the maximum thickness of 1.8 cm. Also, the thickness of the connecting wires is uneven in each coil and varies between each winding.

2.2.3 Computer modelling of non-uniformity of the TH coil prototype windings

Since the H-field of the TH Coil was higher than the calculated value, coil asymmetry and wire attached to the windings were assumed to be the cause for the non-uniformity of the magnetic

field. The connecting wire to the coil must withstand a large current, which is why they have a thick connecting wire, extended to approximate 50 mm along the coil's windings. The positive and ground wire total cover about 100 mm of the coil as shown in Fig. 2-8 running in the opposite directions and causing non-uniformity in the H-field distribution.

Fig. 2-9 presents the H-field along the major axis of the TH Coil, where the measurement and data from the computer simulation are not a good match but they are closely related. The curve shows the data points from the center of the coil towards the coil windings. The effect of the extra connection of the cables can be seen along this axis also, resulting in the deviation in the values of measurement from the calculated value. One of the main difference between Fig. 2-7 and Fig. 2-9 is that the coils are flattened (Fig. 2-8) while taking the measurement for the major and minor axis (Fig. 2-9 & Fig. 2-10). This was taken into consideration to make the system simple and to emphasize on the effect of the cable connections to the coil windings. Furthermore, the simplified model (Fig. 2-11) is a better representation of the TH Coil with flattened coils.

The measurement data along the minor axis is larger than the calculated one (Fig. 2-10) due to the cable connections to the coil windings. The difference in the measurement and calculated data is higher as it moves closer to the windings and decreases at the center of the coil. Since, the cables are connected to one side of the coils, the measured field is unsymmetrical and H-field value is higher on that side.

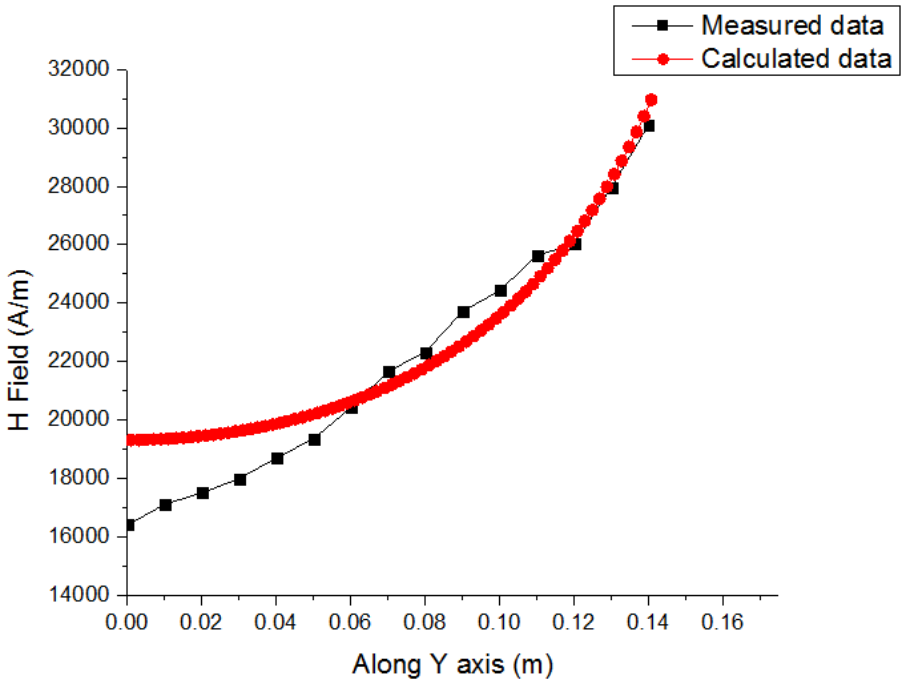

Figure 2-9. H-field along the major axis where the calculated and measured data is not fully comparable.

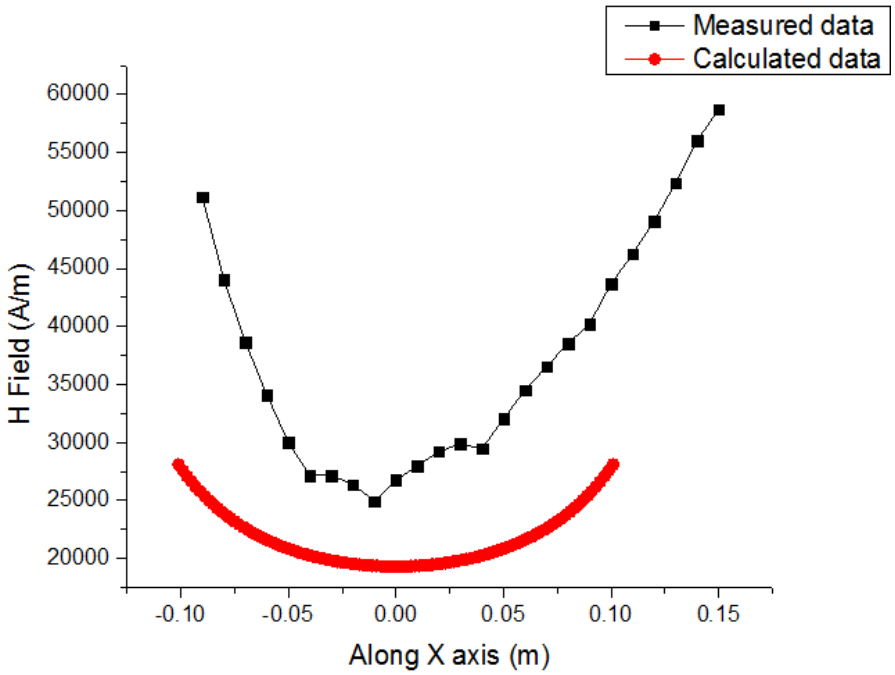

Figure 2-10. H-field along the minor axis where the calculated and measured data is not at all comparable.

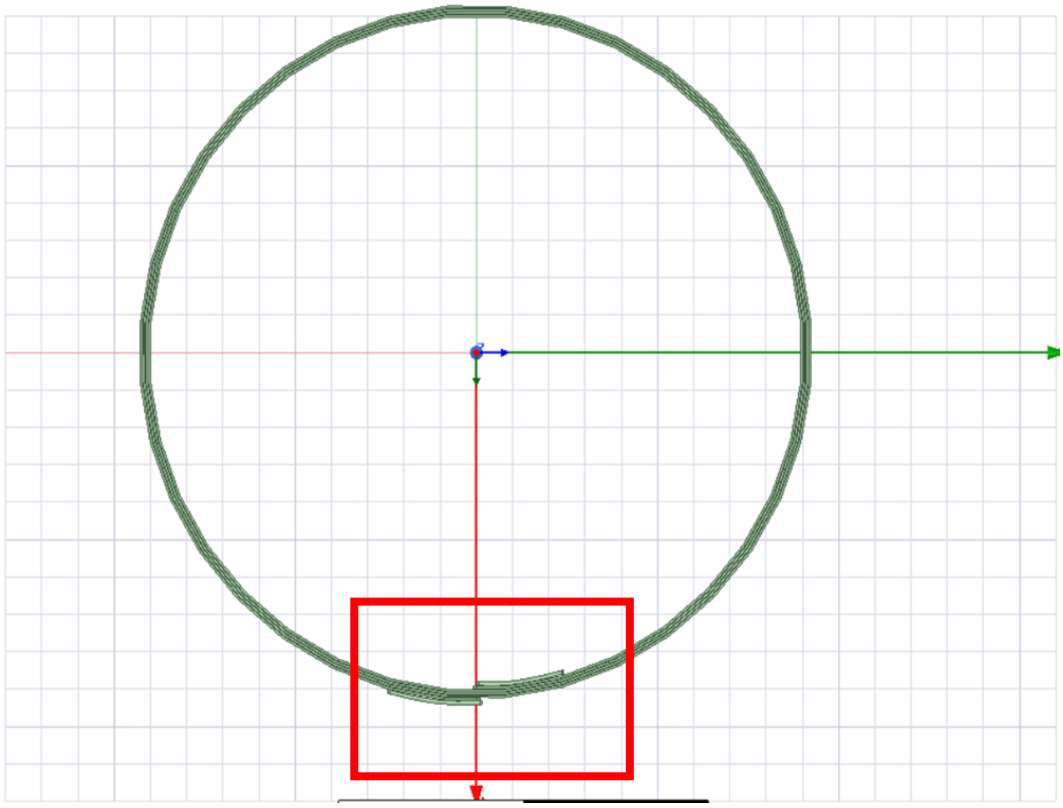

Figure 2-11. Circular coil with four turns modelled with a rectangular wire. The red box shows the extra wire attached to the coil to see the effect of cable connections with the coil windings on the H-field.

A simple model of TH Coil was made (Fig. 2-11) using 3D Maxwell solver, ANSYS Electromagnetic software to determine the reason for the not uniform field along one of the axis. The hypothesis, that the cable connected to the coil is affecting the field has been verified. Maxwell 3D solver is used, due to the low frequency application. The simplified model was constructed utilizing a circular coil instead of an elliptical coil. Only one coil with four windings was used to proof the concept and verified the hypothesis. The dimensions were kept closed to the prototype. The wire was of a rectangular shape with 6.86 by 1.14 mm with the

radius of the coil to be 180 mm, where in actual coil it is 170, 204 mm with minor and major axis respectively.

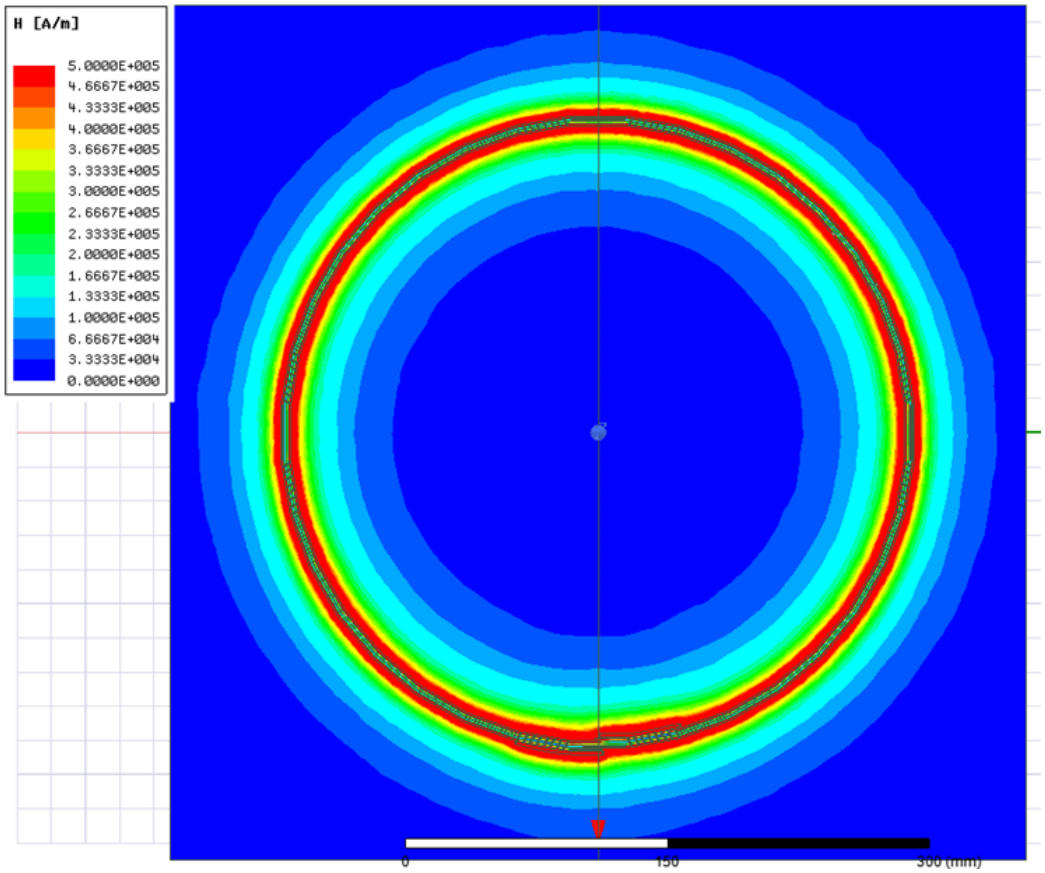

Figure 2-12. H-field along the coil and on the extra connections. The field seems to be more near the cable connections as expected.

The H-field shown by the simplified model (Fig. 2-12) has non-uniform and high magnitude where extra cables are connected as compared to the other parts in the coil. Thus, this simplified simulation proves that the increase in the measured H-field along the minor axis is due to the cable connection to the coil windings.

2.3 Discussion

The TH Coil is able to deliver significantly greater E-Field intensities to deep brain regions than conventional TMS coils. The design of the TH Coil aims to maximize the depth of stimulation, without concern for focality. Because of this, a notable limitation of the presented coil design is that it may only be able to stimulate deep areas while also stimulating superficial areas. Further, the deep areas are stimulated with lesser intensity than superficial areas, but this will be true of any TMS coils because of the rapid decay of the magnetic field.

Because these coils allow stimulation to be adjusted through changes in position/angle, current intensity, current polarity, and combination with secondary coils such as circular or Figure-of-8 coils, the TH Coil is highly flexible, and a diverse set of configurations can be employed to optimize its setup for specific uses. Connections of all three toroids with the Magstim stimulator in parallel reduces the total inductances of the TH Coil configuration to a great extent and increases its power efficacy but at the same time it reduces the current flowing through the coils (1200 A), which should be considered in future uses.

The TH Coil configuration has the potential of stimulating deep brain structures, yet it doesn't have required focality and end up stimulating large portion of the brain. In future, magnetic shields can be used to improve the focality of TH Coil configuration [52][53]. Despite, the drawbacks of the TH Coil configuration, it has the potential to provide an alternative solution to adjust the power level to stimulate deep brain regions without overstimulating the cortex. [54].

2.4 Conclusion

A novel coil configuration called the Triple Halo Coil configuration was designed for deep brain stimulation. Induced E-field was shown at the centered sagittal, centered coronal and several axial plane generated by TH Coil with and without Figure-of-8 coil. Magnetic fields were calculated using a heterogeneous head model when stimulated with different coil configurations such as “Halo Coil”, Figure-of-8 coil and the circular coil and compared with the TH Coil configuration with and without Figure-of-8 coil. We have shown that the novel TH Coil configuration can generate magnetic field that is more than 7 times higher than the Figure-of-8 coil alone at 10 cm from the surface of the head. Furthermore, this new coil design opens the possibilities of treating deep brain neurological disorders by stimulating the deeper regions of the brain.

CHAPTER 3

QUADRUPLE BUTTERFLY COIL: COIL DESIGN WITH IMPROVED FOCALTIY

This chapter has used materials that were published in the paper "Development of Transcranial Magnetic Stimulation Coil Designs with Improved Focality", by P. Rastogi et. al, with the permission of all the authors [72].

In TMS, the shape and size of the magnetic coils plays an important role in determining focality and depth of stimulation in the brain. There have been many coils designed in the last twenty years utilizing different geometrical layouts, but no coils have shown significant improvement in focality over the Figure-of-8 coils while maintaining the field intensity required to stimulate at the depth of the brain. The Figure-of-8 coil configuration was first proposed by Ueno et al. in 1988 and functional mapping of the motor cortex was successfully obtained with a 5mm resolution in 1990 by the same group [15], [55]. Different varieties of the Figure-of-8 coil are FDA approved for the treatment of chronic depression [56]–[58]. But it is not clear that the focal nature of Figure-of-8 coils is what makes them effective at treating depression, because the H-Coil, which allows for deeper and less focal stimulation of the brain, has also proven to be effective at treating depression [59].

In neurotherapeutics, the ideal stimulation site for TMS is unknown and will likely prove to be dependent on the nature of the disease to be treated and also potentially the subject. TMS is still a relatively new technique and there is much that needs to be tested before researchers develop an understanding of what the ideal stimulation parameters are. Any development of TMS coils that allow for stimulation beyond the resolution of Figure-of-8 coils will give researchers more opportunities to stimulate specific neural circuits that are identified to be

important in specific neurological disorders. Further, more precise stimulation methods also limit the modulation of neighboring brain regions whose relationship with a given disease may be unknown or dissimilar to that of the target stimulation site. Beyond therapeutics, as researchers continue to use TMS to explore different physiological measures or concurrent TMS & fMRI (functional magnetic resonance imaging) or TMS & EEG (electroencephalography), more focal stimulation will be desired as it allows for more direct understanding of TMS outcomes.

In this chapter, a new coil design, namely the Quadruple Butterfly Coil (QBC) has been developed with the main purpose of allowing researchers a finer resolution for stimulation. This new coil aims to decrease the stimulation volume over the cortex and not to achieve deeper brain stimulation as highlighted in previous work [41]. The focality term used in this paper refers to the decrease in volume of stimulation due to the QBC when compared with the Figure-of-8 coil. Also, the QBC has been compared with the Figure-of-8 coil using 50 anatomically realistic heterogeneous MRI derived head models that we have developed at ISU. These coils were positioned on the vertex of the head and also on the area of the scalp over the dorsolateral prefrontal cortex.

3.1 Description of computer simulation set-up

The 50 head models (Fig. 3-2) used in this study were developed by Lee et al. [60] using the SimNIBS pipeline, which was utilized to segment anatomical regions from Human Connectome Project MRI images [60]–[62]. These models consist of seven different segmented anatomies including skin, skull, cerebrospinal fluid (CSF), grey matter (GM), white matter (WM), cerebellum and ventricles as shown in Fig.3-1. Also, these models were created

from healthy young adults in the age range from 22-35 years, with an equal number of female and male head models.

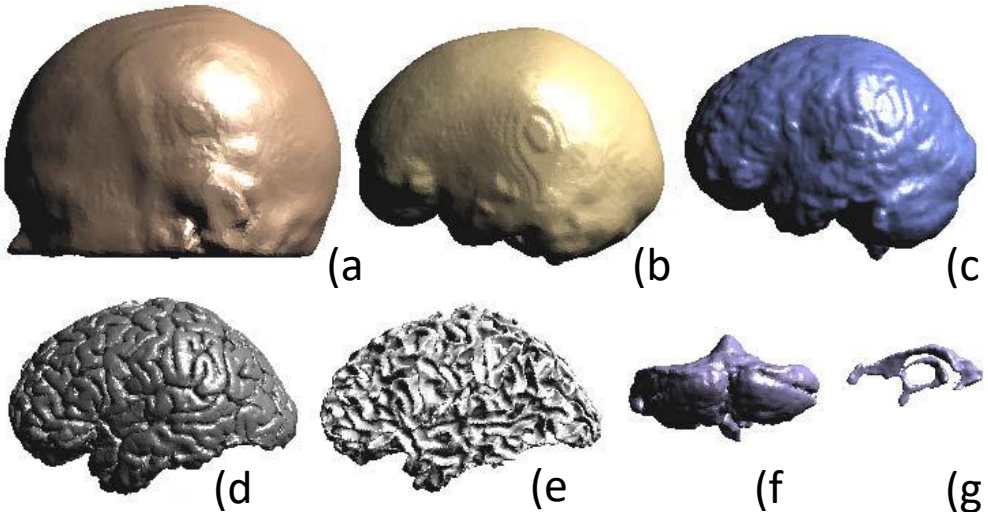

Figure 3-1. Seven different segmentations used in the MRI derived head models (a) skin (b) skull (c) CSF (d) gray matter (e) white matter (f) cerebellum (g) ventricles [42].

Figure 3-2. Top view of all the 50 MRI derived healthy head models used in the computer simulations.

Calculation of the electric field (E-field) and modeling of TMS coils was performed using SEMCAD X [47]. The current supplied to the TMS coils was 5000A peak to peak at a frequency of 2.5 kHz. The corresponding relative permittivity and electrical conductivity values were taken from Hasgall et al. [63]. A quasi-static, low frequency solver was used for the calculation of the induced electric field in the brain and magnetic fields generated from the coils. Results from SEMCAD X were exported to MATLAB for data processing and construction of plots. A Magstim 70mm Figure-of-8 coil was used as a comparison coil for the results with QBC [64]. Results from the Figure-of-8 coil were included in this paper for the purposes of comparison, since this coil has been widely used in TMS literature and is able to provide a reference for the results that is different from the new QBC [65][66].

The QBC is designed with two sets of coils, two larger coils which are the same size as the Figure-of-8 coil, and two smaller coils, which are 40% of the size of the larger coils with an inclination of 45 degrees as shown in Fig. 3-3. QBC geometry, without the additional set of smaller coils, is based on Eaton et al. and highlighted in Deng et al. as a 50mm V-coil [37], [67]. There are equal numbers of windings in both the bigger and smaller coils as in the Figure-of-8 coil, and left and right coils have current flowing in the same direction at the point where the windings are closest, allowing for summation of field intensities. The reason for adding the smaller coils on top of larger coils in the QBC is to increase the magnetic vector potential over the target stimulation site, which is decreased when the coils are angled upwards. This in turn increases the induced electric field in the QBC to be more comparable to that of a Figure-of-8 Coil, while maintaining the increased focality from the angle adjustment. The reason for limiting the size of the second set of coils was to allow the QBC to constrain the increased field intensities to be more centered on the desired target of stimulation. Although increasing the

size of the coils may increase depth of penetration, it also decreases stimulation specificity along the axis defined by the green arrow in Fig. 3-3(a)-(b). There is a limitation for further reduction in the coil dimension because small coils overheat quickly, and it is more difficult to maintain the temperature than in the case of larger coils.

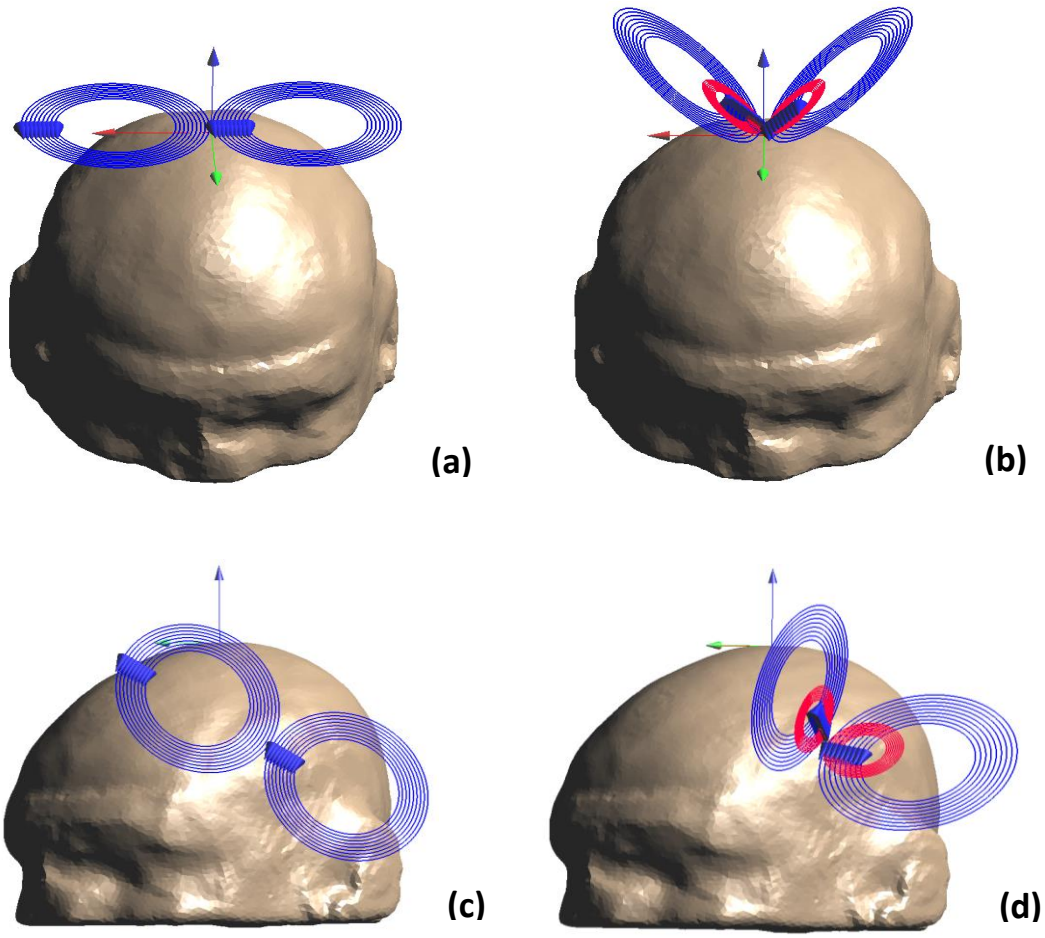

Figure 3-3. Figure-of-8 coil and Quadruple Butterfly Coil positioned (a-b) on the vertex (c-d) on the dorsolateral prefrontal cortex region of the head model.

To compare the simulation results of the two coils at the two test locations, several metrics were employed. These metrics include E-Max (the maximum E-Field intensity in the brain, or other anatomy if specified), V-Half (the volume of the brain exposed to E-Field intensities at

least one half E-Max), distance of E-Max from origin (distance from expected location of E-Max, which is directly below the coil), and A-Half (surface area of the brain exposed to E-Field intensities at least one half E-Max).

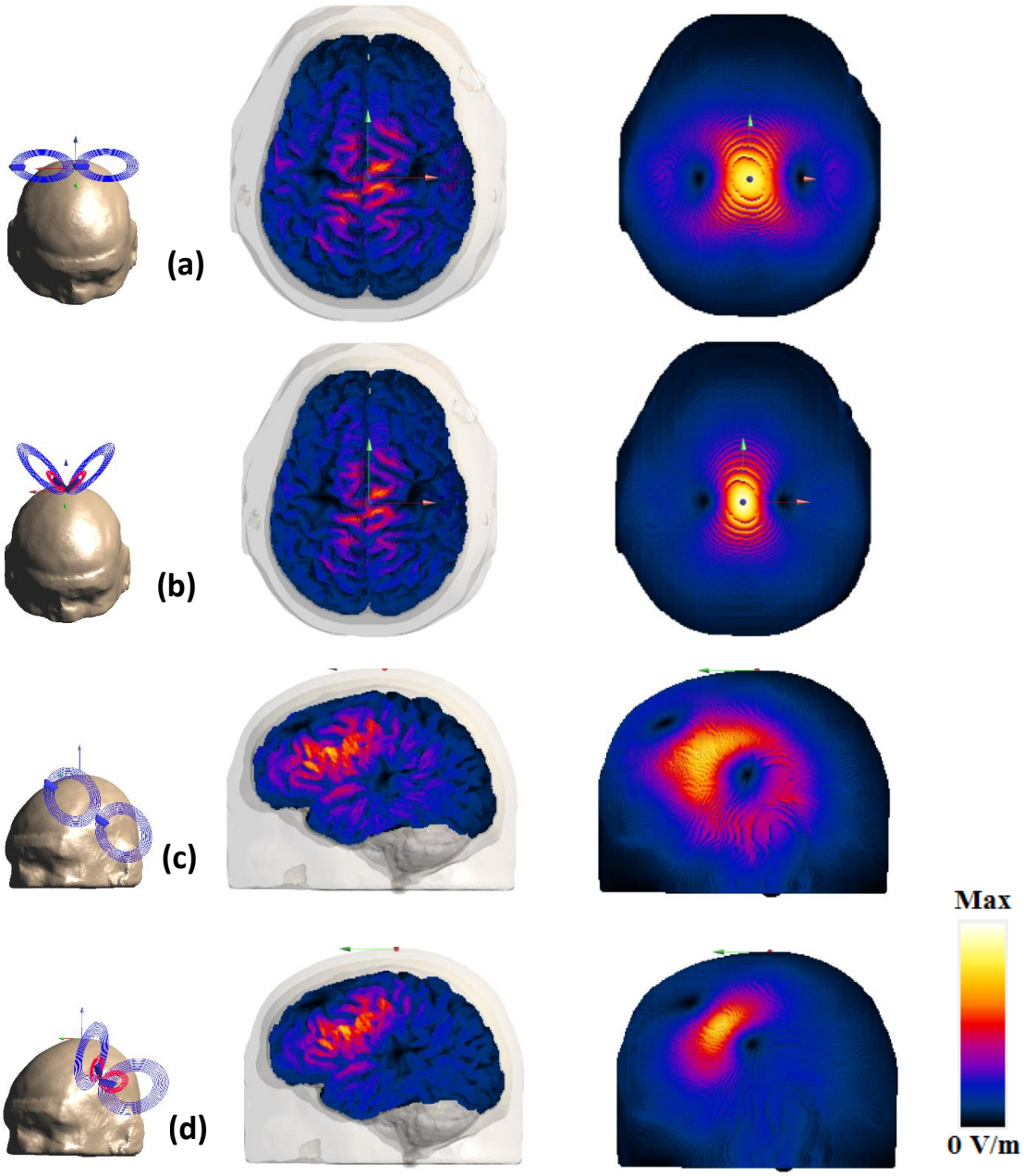

Figure 3-4. Induced electric field on the grey matter and scalp due to (a) Figure-of-8 coil on the vertex (b) Quadruple Butterfly Coil on vertex (c) Figure-of-8 coil on dorsolateral prefrontal cortex (d) Quadruple Butterfly Coil on dorsolateral prefrontal cortex.

3.2 Analysis of the E-field on the 50 head models for QBC and Figure-of-8 coil

The results in this paper show the effect of coil geometry and anatomical variation in brain structure on the 50 head models. Most published research either compares different coil geometries or the effects of anatomical variation, but previous studies have not been able to utilize a broad range of subjects to confirm the potential differences in the stimulation site of different coils [37], [60]. This paper introduces a new coil design, compares its results with the Figure-of-8 coil and also discusses the effect of anatomical variation by using 50 different head models.

In Fig.3-4, the induced electric field on the surface of grey matter (GM) and scalp due to both Figure-of-8 coil and QBC on the vertex and dorsolateral prefrontal cortex is shown. Results in both sets of simulations show increased focality of the QBC towards the direction of the outer coil windings. Further, the images of the E-Field profile on the scalp illustrate that the QBC stimulates a much smaller portion of the scalp than the Figure-of-8 coil. The ability of the QBC to stimulate more focally on the scalp may prove to be advantageous in settings where muscles near the TMS stimulation site are causing excessive twitching in subjects receiving TMS.

The box plot (Fig.3-5), which illustrates three sets of data from Figure-of-8 coil and QBC, shows simulation results with the coils placed only over the vertex of the head models. The first box plot shows the maximum electric field intensity in the brain (E-Max) for all 50 head models due to the Figure-of-8 coil and QBC. The five number summary for E-max (V/m) for Figure-of-8 coil is (114.89 V/m, 158.16 V/m, 191.76 V/m, 213.10 V/m, and 318.08 V/m) and for QBC is (79.78 V/m, 111.17 V/m, 135.94 V/m, 153.12 V/m, and 233.88 V/m).

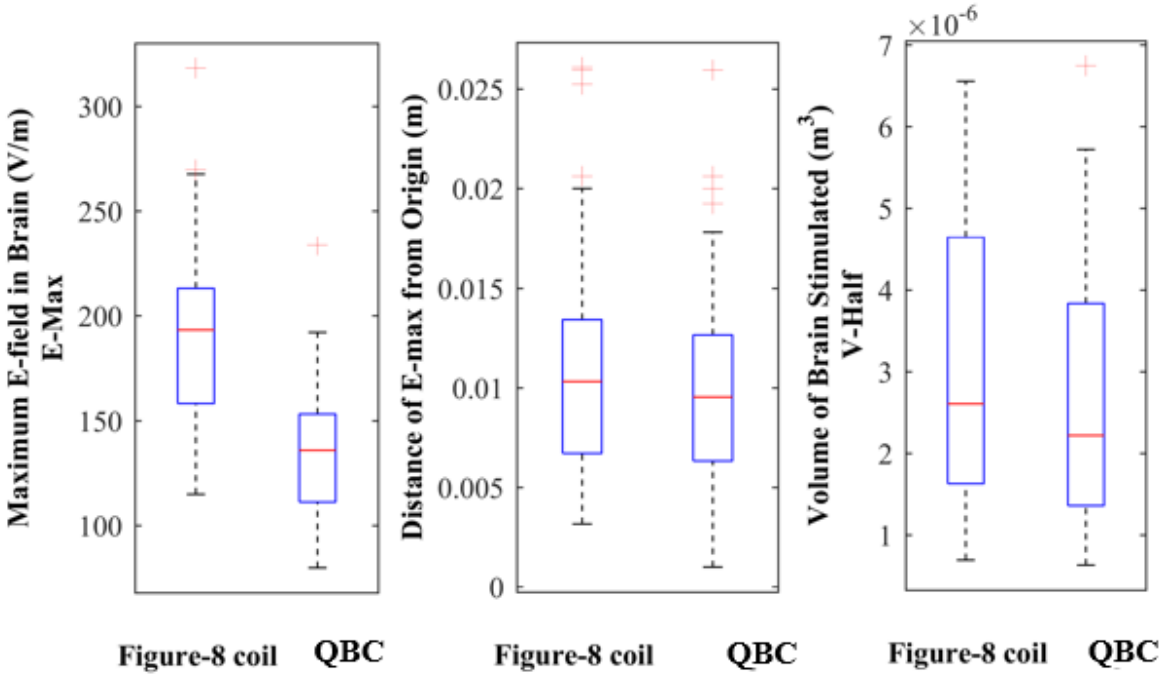

Figure 3-5. Three sets of boxplots showing the five number summary (minimum, first quartile, median, third quartile and maximum, outliers) for E-Max, the distance of E-max from expected location, and V-Half for Figure-of-8 coil and Quadruple Butterfly Coil using 50 sets of head models.

Results show that the QBC stimulates at weaker intensities than the Figure-of-8 coil for a given current intensity, but both coils have a comparable ratio of electric field on scalp to brain (2.17 for QBC and 1.69 for Figure-of-8 at vertex), which is important for not over-stimulating nerves near the site of stimulation. The induced electric field intensity from both coils are sufficient to meet standards which are required for neuronal depolarization [68]. The second box plot illustrates the location of E-Max relative to the expected E-Field maximum (directly below coil). This metric is relevant to understanding the precision of stimulation for different coils. Results show there is a modest improvement of 8 % in the QBC over the Figure-of-8 coil. Similarly, the five number summary for V-Half (m^3) is (6.91e-07, 1.63e-06, 3.02e-06, 4.65e-06, and 6.56e-06) for Figure-of-8 coil and for QBC (6.30e-07, 1.36e-06, 2.67e-06, 3.83e-

06, and 6.74e-06). The third box plot shows a decrease in the volume of the brain exposed to high E-Field intensities (V-Half) by 11.6% while using QBC compared to Figure-of-8 coil, which is a significant reduction in stimulation of brain volume.

Table 3-1. Measures of interest for both QBC and Figure-of-8 coil on two positions.

Measure of Interest (mean)	QBC	Figure-of-8 coil
Coil Positioned at Vertex		
V-Half (m^3)	$2.6709e^{-6}$	$3.0e^{-6}$
E-Max (GM&WM) (V/m)	136	192
Distance of E-Max from Origin (m)	0.0102	0.0111
A-Half (m^2)	0.0010	0.0011
E-Max (Entire head) (V/m)	296	325
Coil Positioned at Dorsolateral Prefrontal Cortex		
V-Half (m^3)	$4.7568e^{-6}$	$5.4481e^{-6}$
E-Max (GM&WM) (V/m)	156	230
A-Half (m^2)	0.0018	0.0021
E-Max (Entire head) (V/m)	282	339

Table 3-1 gives the summary for both positions & coils and gives the means of E-max (on both GM & WM and on Entire head), V-Half, distance of E-Max from expected location of maximum stimulation and area of stimulation. QBC has an advantage over the Figure-of-8 coil in terms of focality and can be used for TMS applications where focality is the main parameter of interest.

Further seen in Table 3-1 is an interesting finding that was not intended to be a main point of this work, but is still necessary to mention. Simulations showed that for a Figure-of-8 coil, the intensity of stimulation is nearly 20% greater over the dorsolateral prefrontal cortex than over the vertex. As most places of interest to TMS researchers are outside of cortical areas that give easily observable physiological responses to indicate what potentially ideal stimulation intensities are, scaling stimulation intensities from motor (aka motor threshold) to non-motor

regions can be a challenge. Future work will need to follow this up in detail for researchers to have a better understanding of how different cortical stimulation sites may require higher/lower stimulation intensities.

3.3 Testing of the QBC prototype

The prototype of the QBC was fabricated by Jali Medicals (Fig. 3-6). Fig. 3-7 shows the transparent top view of inside assembly of the four coils of the QBC. All the four coils were made from the rectangular copper wire with the slight difference in the dimensions for the bigger and smaller coils. The dimensions of the rectangular copper wire for the bigger coil were 0.05 by 0.2 inches and 0.045 by 0.27 inches for the smaller coil with 13 turns in each coil. The smaller coils are placed in such a way that the highest point of the smaller coil is positioned at the center of the bigger coil (Fig. 3-7).

Figure 3-6. Top view of the fabricated prototype of QBC.

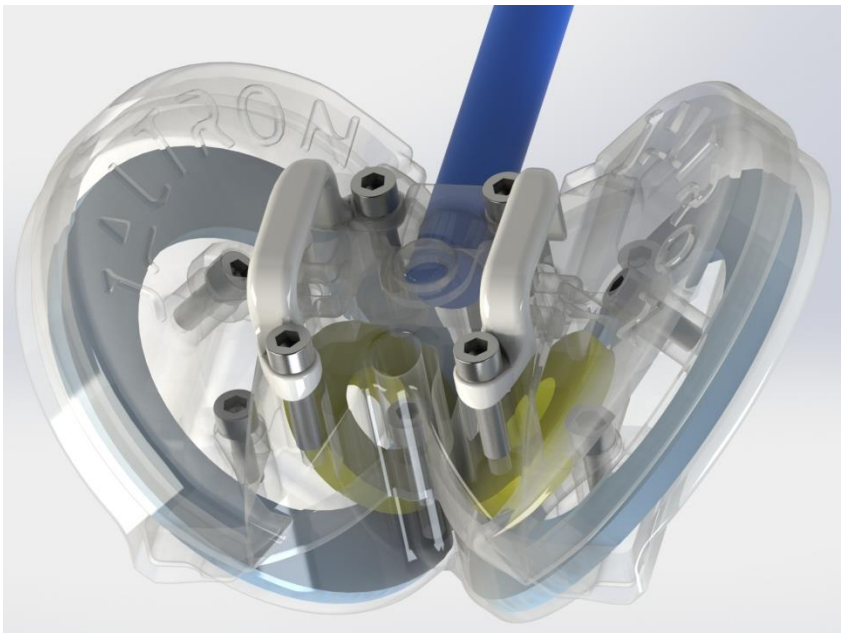

Figure 3-7. Transparent top view of QBC prototype to illustrate the internal windings and connections.

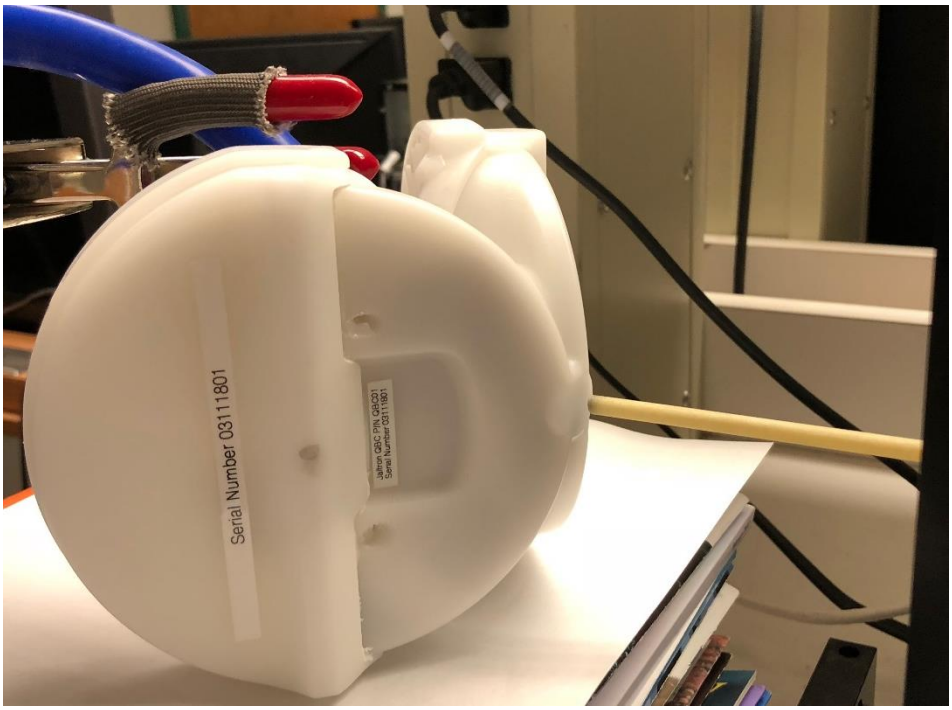

Figure 3-8. Test setup of QBC with a gaussmeter axial Hall probe, positioned at the center of the coil.

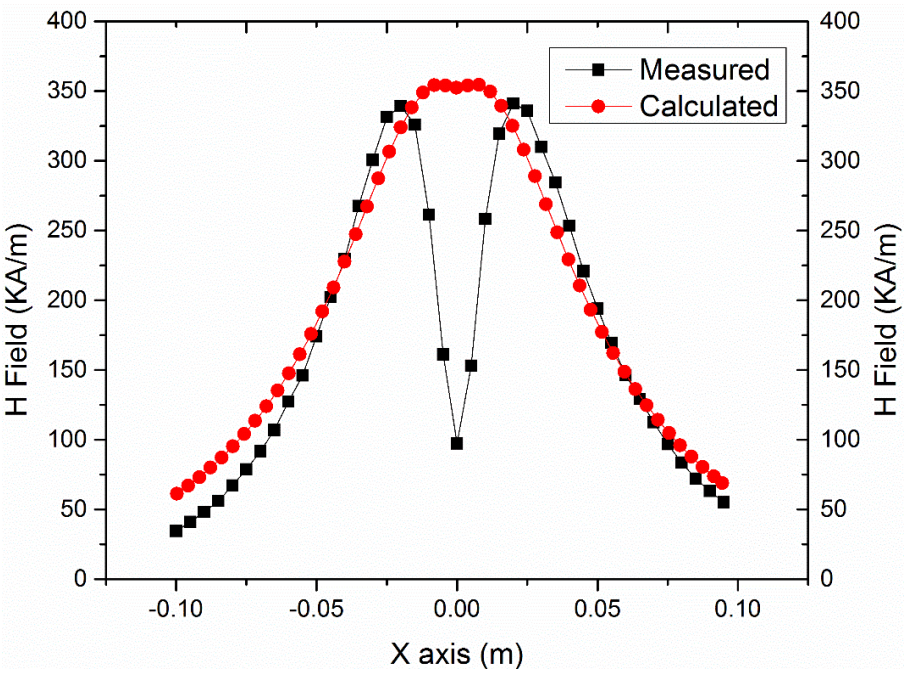

Figure 3-9. Comparison of magnetic field measurement data using gaussmeter and axial hall probe and simulation data along the X axis of the QBC.

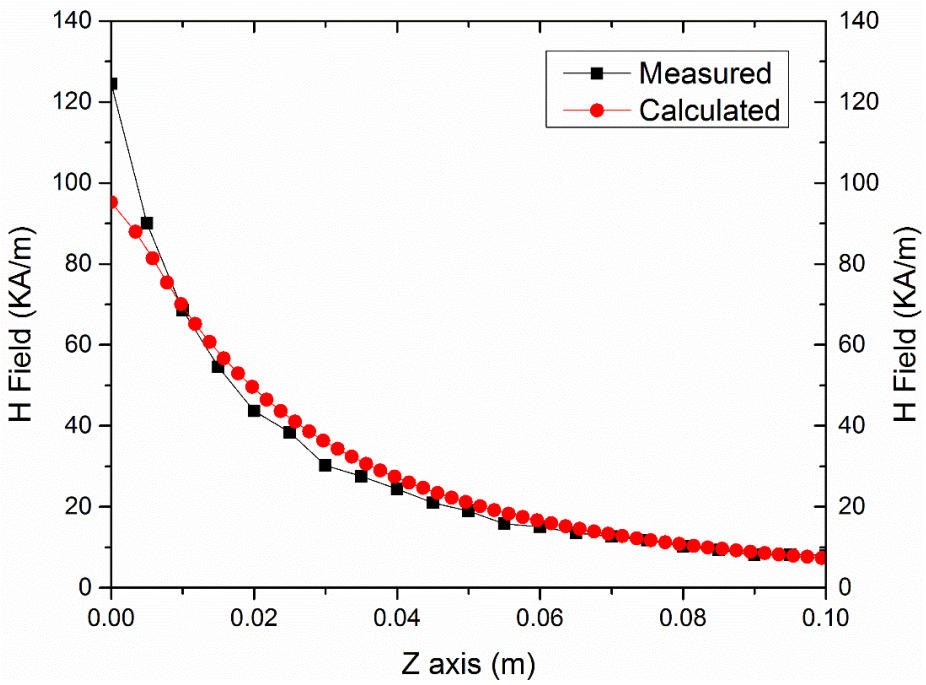

Figure 3-10. Comparison of magnetic field measurement data using gaussmeter and axial hall probe and simulation data along the Z axis of the QBC.

The minimum and maximum diameter of the bigger coil is 70.6 mm and 111 mm respectively and 19.5 mm and 44.5 mm for the smaller coil. The coil also has two small handles (Fig. 3-6) to aid in positioning it at the desire location on a phantom.

For the testing of the QBC, the same measurement system was used as in the Triple Halo coil. The position of the axial Hall probe at the center of the QBC is illustrated in Fig. 3-8. Measurement of the QBC are taken along two directions. When the axial probe moves away from the coil perpendicularly (Fig. 3-8) then the measurements are labelled as “along Z axis” and when the axial probe from the center to the end of the both the coils then it is labelled “along X axis”. The graph showing the measured H-field and calculated H-field using a finite element tool values along the Z and X axis are shown in Fig. 3-9 and Fig. 3-10. The calculated and measured data of H-field shows excellent agreement for both the measurements.

The TMS stimulator has been kept at 100% power level while taking the measurement which is equivalent to 2500 A of current in each coil. Since, there are two pairs of coils (one big and one small coil) in the QBC, the current is halved from 5000 A. The parallel connections of the coils were made to keep the inductance low which is a requirement for the Magstim commercial biphasic stimulator. To keep the same parameters, 2500 A of current was given in each coil in computer modelling.

The measurement probe was approximately 10 mm away from the coil windings due to the plastic insulation and air gap along the X axis. The same distance is considered while taking the simulation data to ensure fair comparison between the two. It can be seen that there is a significant difference between the measured and calculated H-field along the X axis at the very center of the QBC. The values are in a good agreement as the probe moves away from the center to either side. This is a similar pattern which was observed in the measurement of

various Figure-of-8 coils [69]. According to the author, this variation is due to the over estimation of the H-field by the finite element tool when the coils with the opposite current flowing through them are placed together to increase the H-field between them.

For the graph along the Z axis, necessary adjustment has been made while plotting the Fig. 3-10. The calculated data was adjusted by 20 mm to remove the over estimation by the finite element tool.

The maximum value of the measured H-field was 350 A/m, which was close to 25 mm to each side from the center of the coil (Fig. 3-9). The magnetic field pattern is similar to these measured in various Figure-of-8 coils [69]. Here the comparison between the QBC and Figure-of-8 coil has been made due to the similar geometry in the coil shapes. The maximum value of H-field along the Z axis is close to 120 KA/m which is similar to the value measured along the X axis.

Hence, the testing of the QBC prototype was completed successfully and the results were in a good agreement with the computer simulation.

3.4 Conclusion

In this chapter, a novel coil design, the QBC, is proposed, which has modest improvements in focality over the Magstim 70mm Figure-of-8 coil. The QBC has been positioned at two different locations on the head and the TMS induced stimulation profile was calculated for 50 different head models. This work outlines the first major version of the QBC followed by the testing of the QBC prototype which was manufactured by Jali Medicals under the supervision of Dr. Reza Jalinous. The next chapter is about the use of magnetic shields with the QBC to further improve the focality of the coil.

CHAPTER 4

INVESTIGATION OF SHIELDING MATERIAL IN QUADRUPLE BUTTERFLY COIL

This chapter has used materials that were published in the paper "Quadruple Butterfly Coil with Passive Magnetic Shielding for Focused Transcranial Magnetic Stimulation", and "Investigation of shape, position, and permeability of shielding material in quadruple butterfly coil for focused transcranial magnetic stimulation" by P. Rastogi et. al, with the permission of all the authors [52-53].

TMS coil geometry plays an important role in determining the extent and strength of stimulation. Different coil designs enable researchers to have a degree of flexibility with regard to the field profile and in turn the properties of the induced site of stimulation. For TMS, focality and depth of penetration are inversely proportional and this trade-off is difficult to overcome due the rapid decay of the magnetic field with respect to distance from the coil. There are some coil geometries which improve the focality and others which improve depth of penetration of the electric field inside the brain, for treating disorders that originate from deeper regions of the brain [37].

Focal coils have the potential to increase the stimulation delivered to the desired target region while decreasing the stimulation to neighboring regions. These coils may also reduce the electric field in the scalp which can causes discomfort to patients [70]. Potential reduction in peripheral nerve stimulation could allow researchers to stimulate in new areas where excessive nerve stimulation negatively impacts tolerability of treatment.

The authors proposed a novel coil design, the Quadruple Butterfly Coil (QBC), in chapter 3 that aimed to improve the focality of a Figure-8 coil while maintaining a sufficiently strong field to stimulate the brain [64], [71], [72]. In this chapter, we show further improved focality

of a QBC by using a high permeability ferromagnetic material as a passive magnetic shield along with the QBC configuration. Initially, the results of the QBC with a shield are compared with the QBC and the Figure-8 coil using 50 anatomically realistic heterogeneous MRI derived head models when stimulated at two regions of the brain: the vertex and the dorsolateral prefrontal cortex (DLPFC). Single and double shields are used with the QBC to evaluate the effect of the shield on focality. The DLPFC was chosen for stimulation based on its clinical use in TMS for treating depression [73] and the vertex was also included to provide a second anatomical data point for coil performance. DLPFC is situated in the primary cortex region of the brain, which is connected to the regions including orbitofrontal cortex, thalamus, hippocampus, and parts of basal ganglia. Functions of DLPFC includes working memory, planning, abstract reasoning, cognitive flexibility, motor planning, organization and regulation.

Furthermore, in the second half of the chapter, the authors have explored a variety of passive ferromagnetic magnet shield shapes, positions, and permeabilities to improve the focality of stimulation with the QBC. A heterogeneous healthy head model derived from MRIs has been used for all the simulations focused on the vertex of the head to investigate the effects of different shields with the QBC. Several shields of different shapes and sizes have been examined with both the QBC at the vertex and on the area of the scalp over the DLPFC.

4.1 Computer Simulation Setup of QBC with a passive magnetic shield

The analysis of resulting stimulation profiles for the two shield designs is conducted over the 50 head models which were developed by Lee *et al*. by segmenting anatomical regions of MRI images from the Human Connectome Projects, using the SimNIBS pipeline [60]. Sim4life, a finite element analysis tool has been used for modelling of the coil system and calculation of electric and magnetic fields in different tissues of the brain [48]. Sim4life is the

updated version of SEMCAD X and was used in this publication because of its ability to incorporate ferromagnetic materials into simulations. Since SEMCAD X was used in our previous publication, identical simulations were calculated on both Sim4Life and SEMCAD X platforms and results were assessed to show that they gave the same results between platforms before continuing with Sim4Life [47]. In our simulations, the current and frequency applied to the coils was 5000 A and 2500 Hz, respectively. There are two solvers used for the modelling, one for the shield, and the other for the coils and head model. A magnetostatic vector potential solver was used for the shield calculation and a quasi-static, low frequency solver was used for the coils. The electrical conductivity and relative permittivity of different tissues in the head model were assigned based on the existing literature [60][63]. Data from Sim4life was exported to MATLAB for the post-processing analysis of the parameters of interest. Origin software has been used for plot constructions. Results for the parameters of interest from the Magstim 70 mm Figure-8 coil and QBC from the previous publication were included in Table 2 for comparison [71].

The ferromagnetic material used as a passive shield aimed at improving the focality of stimulation is Mu-metal which is positioned in between the head model and the QBC. This shield is in the shape of a semi-circle with a thickness of 3 mm and inner and outer diameters of 48 mm and 60 mm respectively as shown in the Fig. 4-1. Also, the distance between the head model and shield is approximately 2.5 mm and the distance between the head model and coil windings is 5 mm as illustrated in Fig. 4-1.

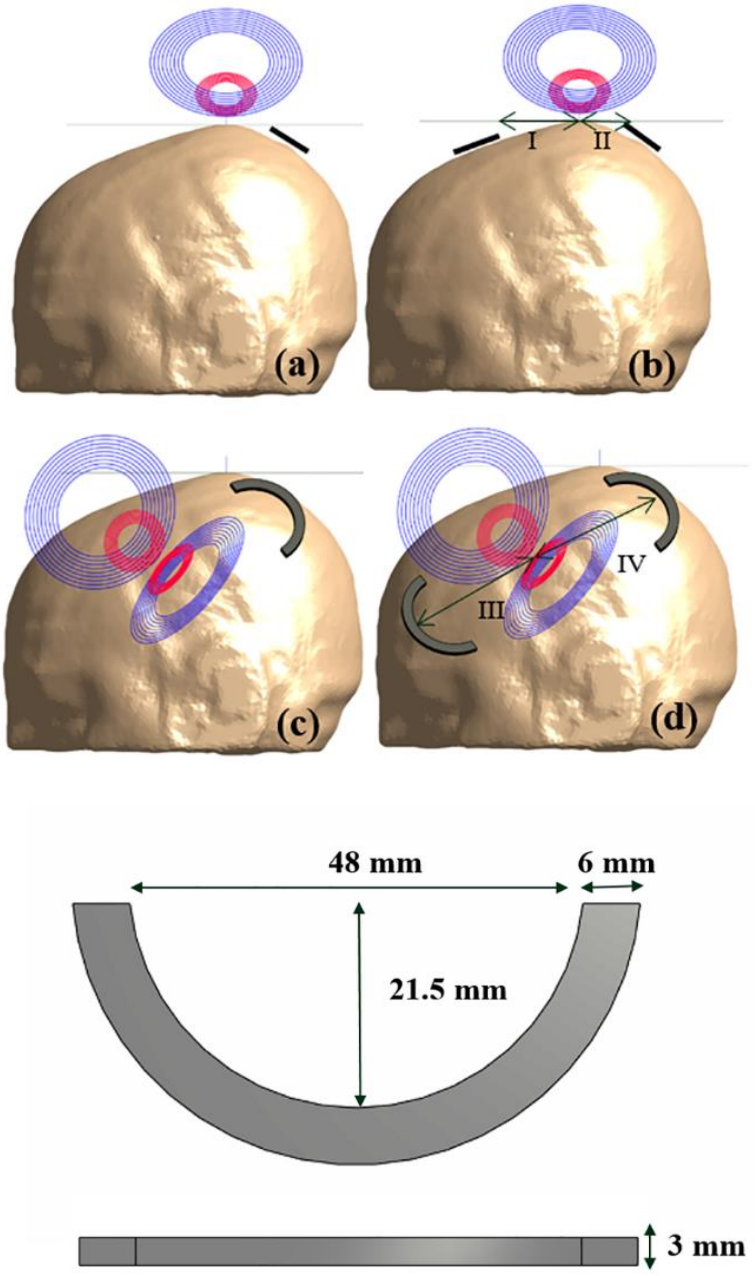

Figure 4-1. The QBC on the vertex position for a particular head model with (a) single shield (b) double shield (I = 52 mm and II = 27.5 mm) and on the dorsolateral prefrontal cortex with (c) single shield (b) double shield (III = 80 mm and IV = 85 mm). Shield dimensions are illustrated at the bottom of the figure.

Furthermore, the shield is rotated along the Y axis by an average of thirty degrees to position it along the scalp for each individual head model. Since, Sim4life only supports one value of relative permeability, it is assigned to be 50,000 for shielding a high magnetic field generated by the QBC. The shields were positioned in such a way so that they were far enough from the coil's center to have small effects on the maximum stimulation intensity, while still being close enough to affect coil focality.

The same parameters of interests as in Rastogi *et al.* [71] were employed such as E-Max brain (the maximum E-Field intensity in the brain – Grey matter &White matter), A-Half (surface area of the brain exposed to E-Field intensities at least one half E-Max), V-Half (the volume of the brain exposed to E-Field intensities at least one half E-Max), and E-Max head (the maximum E-Field intensity in the entire head) for the analysis of the results on all 50 head models [71].

For the analysis of different shapes, position, angle and permeability an average head model for the simulations over the vertex position and four more head models for the simulations over the dorsolateral prefrontal cortex position were chosen by a random number generator from a set of 50 head models [60].

4.2 Analysis of the results due to QBC with a shield

Few publications have reported on the use of shields together with TMS coils in spite of the advantage they provide by improving the focality [37][74]. Kim et al. improved the focality of the Figure-8 coil by using a conductive shield plate [74]. In this dissertation, we are trying a similar approach but with a ferromagnetic material with the help of different shield shapes.

Initially to access the effect of shield along with QBC configuration, a semi-circle shape of the shield was chosen because this shape helps to reduce the magnetic field in the surrounding

region without affecting the primary region of interest. Furthermore, the curved shape of the shield directed the magnetic field vectors toward the region of interest. Simulation results show no significant difference in the mean value of E-Max when compared to the QBC alone although there is a significant improvement in focality. An important advantage of the QBC is the angular shape which helps in positioning the shields below the QBC coils without increasing the distance between the coil and scalp. This is not possible with the Figure-8 coil configuration, since the windings of the Figure-8 coil are all in one plane, and placing the shield between the head and coil will increase the gap between them. The E-Max gets reduced with increase in the distance between the head and coil due to the decaying property of the magnetic field.

Table 4.1 Five number summary of V-half due to the QBC with single and double shields

V-Half (m^3)	Vertex	Dorsolateral prefrontal cortex
QBC with single shield		
Minimum	1.3290E-07	2.9271E-07
First Quartile	1.0638E-06	2.9699E-06
Median	1.9205E-06	3.8905E-06
Third Quartile	3.4065E-06	5.9752E-06
Maximum	8.4110E-06	7.3140E-06
QBC with double shield		
Minimum	1.3194E-07	2.9638E-07
First Quartile	1.0987E-06	2.9693E-06
Median	1.9024E-06	3.9237E-06
Third Quartile	3.2419E-06	5.9724E-06
Maximum	7.9240E-06	7.3120E-06

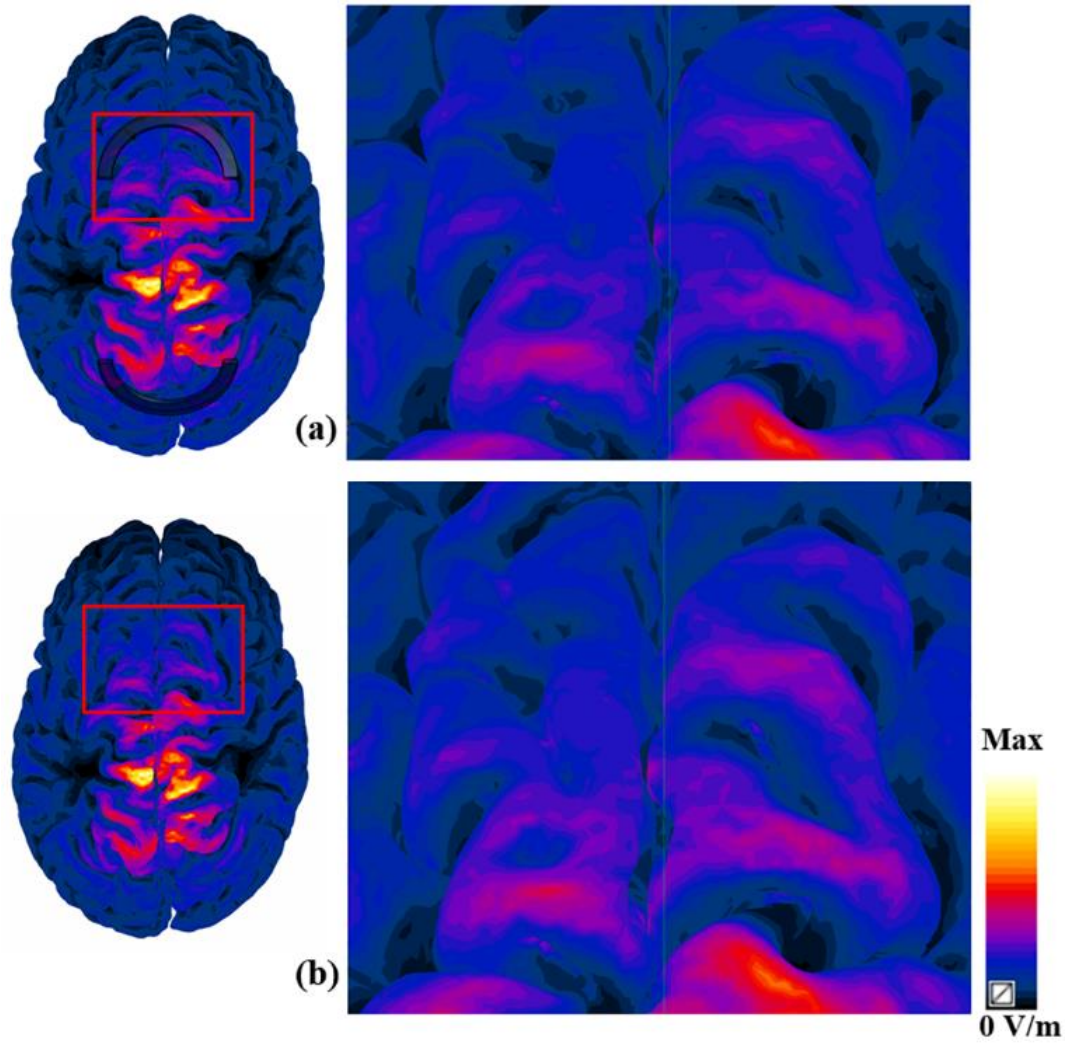

Figure 4-2. Position of the shield and induced electric field on the grey matter and due to the QBC on vertex with (a) double shield (b) no shield and zoomed in image on the right side.

Table 4-2 explores the effects of both one and two shields with the QBC for both stimulation locations and all 50 head models. Simulation results outline a decrease in the V-Half of the QBC with single shield (at the vertex position) by 11.7% and by 13.4% with double shield from QBC alone. Also, a 21.4% (single shield) and 22.9% (double shield) decrease in the V-Half when compared to a commercial Figure-8 coil, making a significant improvement in the focality.

Furthermore, a decrease of 14.4% in V-Half (at prefrontal position) due to the QBC with both single and double shield, when compared to the QBC alone followed by 25.3% (single and double shield) decrease in V-Half when compared with the Figure-8 coil. Further details of the V-Half are provided by Table 4-1.

Table 4-2. Parameters of interest due to QBC with one shield and QBC with two shields.

Coil and position	Parameters of Interest	Values (Mean)
QBC with single shield at vertex	V-Half (m^3)	2.36E-6
	E-Max (GM&WM) (V/m)	138
	E-Max (Entire head) (V/m)	257
	A-Half (m^2)	0.0010
QBC with double shields at vertex	V-Half (m^3)	2.31E-6
	E-Max (GM&WM) (V/m)	136
	E-Max (Entire head) (V/m)	256
	A-Half (m^2)	0.0010
QBC with single shield at prefrontal cortex	V-Half (m^3)	4.07E-6
	E-Max (GM&WM) (V/m)	162
	E-Max (Entire head) (V/m)	237
	A-Half (m^2)	0.0016
QBC with double shields at prefrontal cortex	V-Half (m^3)	4.07E-6
	E-Max (GM&WM) (V/m)	161
	E-Max (Entire head) (V/m)	237
	A-Half (m^2)	0.0016

E-Max (GM&WM): the maximum E-Field intensity in the brain,
E-Max (Entire head): the maximum E-Field intensity in the entire head,
A-Half: surface area of the brain exposed to E-Field intensities at least one half E-Max,
V-Half: the volume of the brain exposed to E-Field intensities at least one half E-Max.

The ratio of electric field on scalp to brain at the dorsolateral prefrontal cortex is 1.80 for the QBC alone, 1.46 for a single shield, 1.47 for a double shield and 1.47 for the Figure-8 coil. This ratio is an important parameter for determining the stimulation of nerves on the scalp. Interestingly, this change in ratio is representative of a decrease in stimulation intensities at the scalp, while the maximum intensities observed in the brain are not affected. This reduction is around 40 V/m from QBC alone to QBC with shields.

Fig. 4-2 illustrates the decrease in the induced electric field in the grey matter of a head model with the use of shields with the QBC. The magnified area of the grey matter near the shield shows the decrease in the area of stimulation near the regions where shield has been placed.

A histogram of the E-Max in the brain is shown in the Fig. 4-3 for both the positions, and for QBC with and without shield/shields for all 50 head models. Both the histogram plots are slightly skewed to the right. There is an outlier in the Fig. 4-3 (b), as this model has less brain to scalp distance and because there was a high field in the grey matter. It was also found that there was a large electric field intensity in an unexpected, isolated region of the brain which is likely to be a numerical artifact [75].

As stated before, there is no difference in the E-Max of the QBC with a single or double shield, but models close to the mean value have greater values of E-Max for QBC with shields in comparison to the QBC alone. Although, this trend does not hold true as the value moves away from the mean (Fig. 4-3).

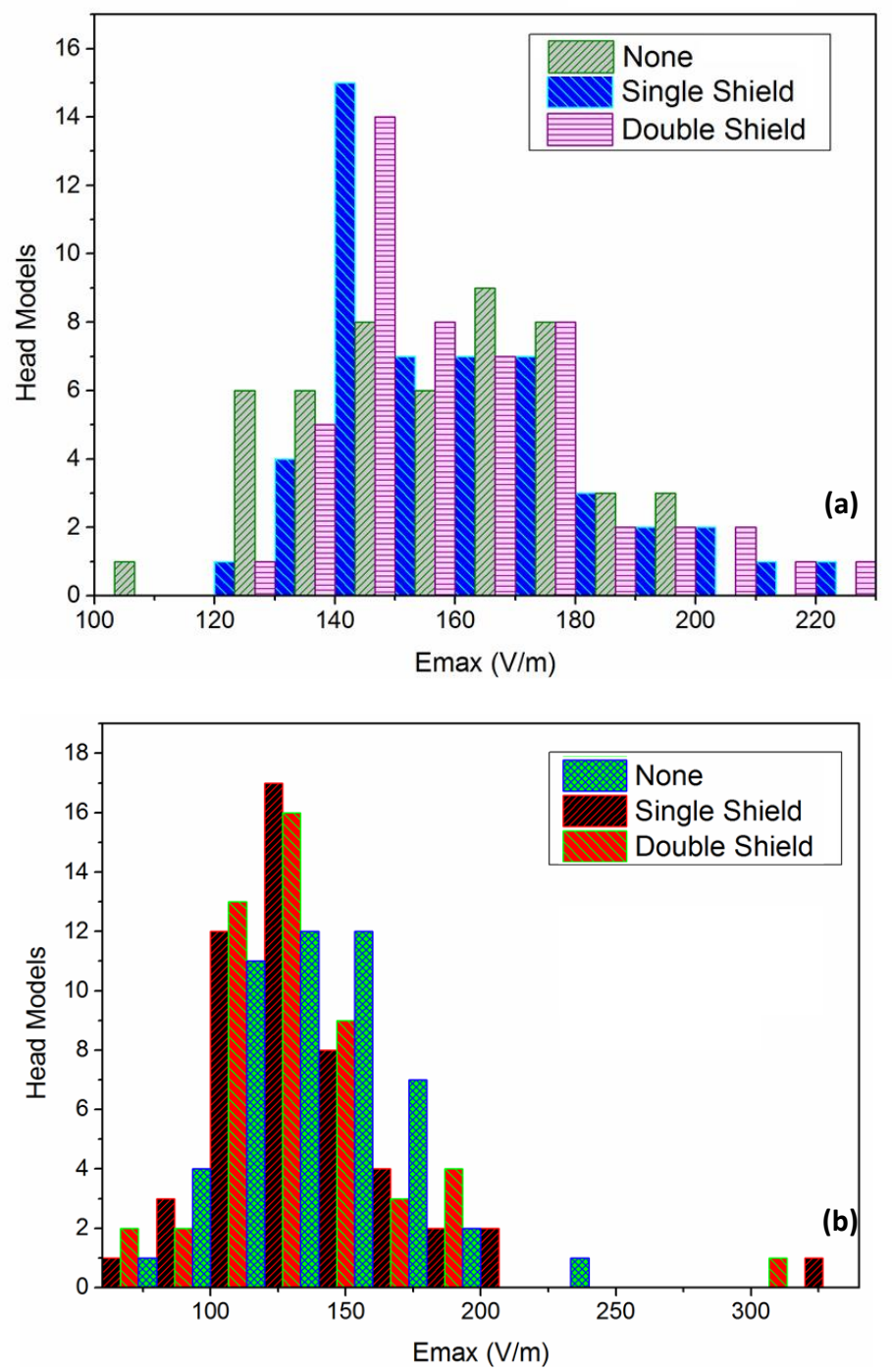

Figure 4-3. Histogram of maximum electric field in the brain due to the QBC on the (a) dorsolateral prefrontal cortex and (b) vertex region with single shield, double shield and the QBC alone on the 50 head models. It shows the distribution of E-Max for different coil configurations in the 50 head model population.

Further details about how the magnetic field has been shaped by the addition of a magnetic shield is shown in the Fig. 4-4. Magnetic field vectors are shown along the transverse and sagittal plane for the coil positioned at the vertex and the dorsolateral prefrontal cortex, respectively. By the presence of the shield, magnetic field vectors which were going away from the brain are rotated towards the brain. Also, the value of the magnetic field vector is large due to the use of ferromagnetic material for the shielding. In Fig. 4-4(b), it is shown that field vectors inside the right corner of the red box were going away from the head in the absence of the shield, where as they are rotated towards the brain by few degrees in the presence of a shield.

The double shield was not shown to be advantageous over the single shield at the dorsolateral prefrontal cortex. One of the reasons the second shield did not improve results over the dorsolateral prefrontal cortex is the shape of the head. When the QBC was positioned over the dorsolateral prefrontal cortex, the second shield was away from both the coil and head to keep the shields parallel to each other which was one of the reasons for no improvement in the results. Also, when shields are placed close to the coils, they reduce the E-Max at the target location which is not desirable.

4.3 Analysis of the results due to QBC with varying permeability, shape and position of magnetic shields

4.3.1 Permeability

In this subsection, we have changed the permeability of the shield while keeping all other variables constant: position of the shield, distance of the shield and shape of the shield. The permeabilities tested range from 25,000 – 95,000, representing a “soft” ferromagnetic material.

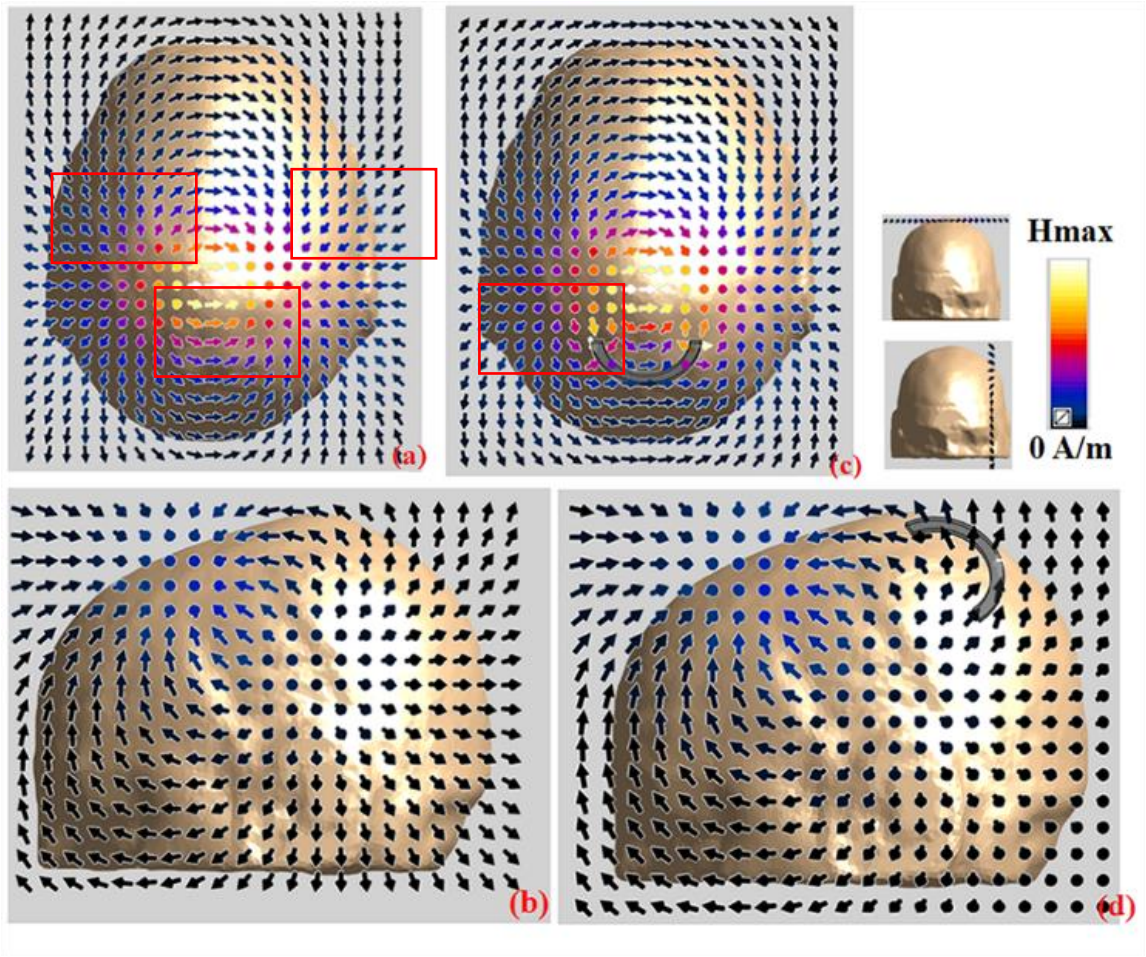

Figure 4-4. Vector field view of the magnetic field on the vertex (a) without shield (c) with shield and on the dorsolateral prefrontal cortex (b) without shield (d) with shield. On the right side of the figure, location of the plane is shown on the head model.

It can be seen that permeability has not resulted in any significant change in the focality, which could have been limited by the range of the permeabilities value taken into consideration. This can be seen as the volume and area that receive high stimulation intensities remain fairly constant as shown in Table 4-3.

Table 4-3: Varying the value of the permeability of the shield.

Permeability	E-Max (GM &WM) V/m	E-Max (Entire Head) V/m	V-Half (GM &WM) m^3	A-Half (GM &WM) m^2
25000	141.78	259.06	1.8E-06	7.14E-04
30000	141.77	259.05	1.8E-06	7.14E-04
35000	142.08	258.56	1.84E-06	7.23E-04
40000	142.93	259.98	1.87E-06	7.35E-04
45000	142.92	259.97	1.87E-06	7.35E-04
50000	141.92	258.92	1.85E-06	7.30E-04
55000	142.02	258.92	1.82E-06	7.18E-04
60000	141.92	258.92	1.85E-06	7.30E-04
65000	142.02	258.92	1.82E-06	7.18E-04
70000	141.74	259.02	1.79E-06	7.14E-04
75000	142.02	258.92	1.82E-06	7.18E-04
80000	142.01	258.92	1.82E-06	7.18E-04
90000	142.01	258.92	1.82E-06	7.18E-04
95000	141.91	258.91	1.85E-06	7.30E-04

4.3.2 Thickness of the shield

In this subsection, the permeability = 50,000 (keeping the value same as before) and only the thickness of the shield is varied while keeping the other parameters constant. The thickness of the shield has been increased in such a way that the distance between the shield and the scalp has remained constant. Increasing the thickness of the shield decreases the E-Max and V-Half proportionally. The thickness of the shield is varied from 1 mm to 10 mm. This does little to help improve the focality of stimulation as shown in Table 4-4.

Table 4-4: Varying the thickness of the shield.

Thickness mm	E-Max (GM &WM) V/m	E-Max (Entire Head) V/m	V-Half (GM &WM) m^3	A-Half (GM &WM) m^2
1	143.2799	259.96	1.86E-06	7.41E-04
2	142.6345	259.14	1.85E-06	7.26E-04
3	141.9229	258.92	1.85E-06	7.30E-04
4	141.5923	257.96	1.82E-06	7.15E-04
5	140.7419	257.08	1.82E-06	7.14E-04
6	140.5145	256.80	1.81E-06	7.11E-04
7	140.0364	256.27	1.78E-06	7.02E-04
8	139.7844	255.97	1.79E-06	7.05E-04
9	139.2232	255.19	1.78E-06	7.05E-04
10	140.0895	256.41	1.82E-06	7.14E-04

4.3.3 Distance of the shield from the scalp

Distance of the shield from the scalp has been varied while the other parameters were kept constant. This includes the position of the coil itself. Since the QBC is conical in shape, the shield can be shifted vertically without having to move the QBC. Seeing as the shield is moving progressively closer to the coil as it moves away from the scalp the interaction between the QBC and the shield increases. This is apparent, as the E-Max has increased 4 % as the distance from the scalp increases (Table 4-5). This may prove to be useful when the desired field is not met even after the power level is at its maximum output, the shield can then be shifted to increase the induced E-Max.

Table 4-5: Varying the distance of the shield from the scalp.

Distance between shield and scalp (mm)	E-Max (GM &WM) V/m	E-Max (Entire Head) V/m	V-Half (GM &WM) m^3	A-Half (GM &WM) m^2
1	141.76	259.03	1.79E-06	7.14E-04
3	142.32	259.51	1.84E-06	7.23E-04
5	142.92	259.97	1.87E-06	7.35E-04
7	143.45	260.39	1.86E-06	7.40E-04
9	143.94	260.65	1.94E-06	7.61E-04
11	144.51	260.96	1.95E-06	7.62E-04
13	144.83	261.56	2.01E-06	7.80E-04
15	145.60	262.09	2.00E-06	7.79E-04
17	146.20	262.85	2.01E-06	7.85E-04
19	146.62	263.28	2.03E-06	7.93E-04
21	147.29	263.71	2.04E-06	7.99E-04
23	147.52	264.05	2.07E-06	8.07E-04

4.3.4 Different shapes of the shield

We have also investigated shield geometry and position of the shield with respect to the coil while holding the permeability constant = 50,000. There are three different shapes of the shield which have been explored: (a) V-shape, (b) Brick, and (c) Two Semicircles as shown in Fig. 4-5. Each of which was placed on both the vertex and DLPFC position of the head model. The exact placement of the shield with respect to the coil and scalp can be seen in Table 4-6. The chosen arc angle of the V shape and semicircles of the shields are the results of several simulation iterations for obtaining the maximum E field value and reduced volume of stimulation.

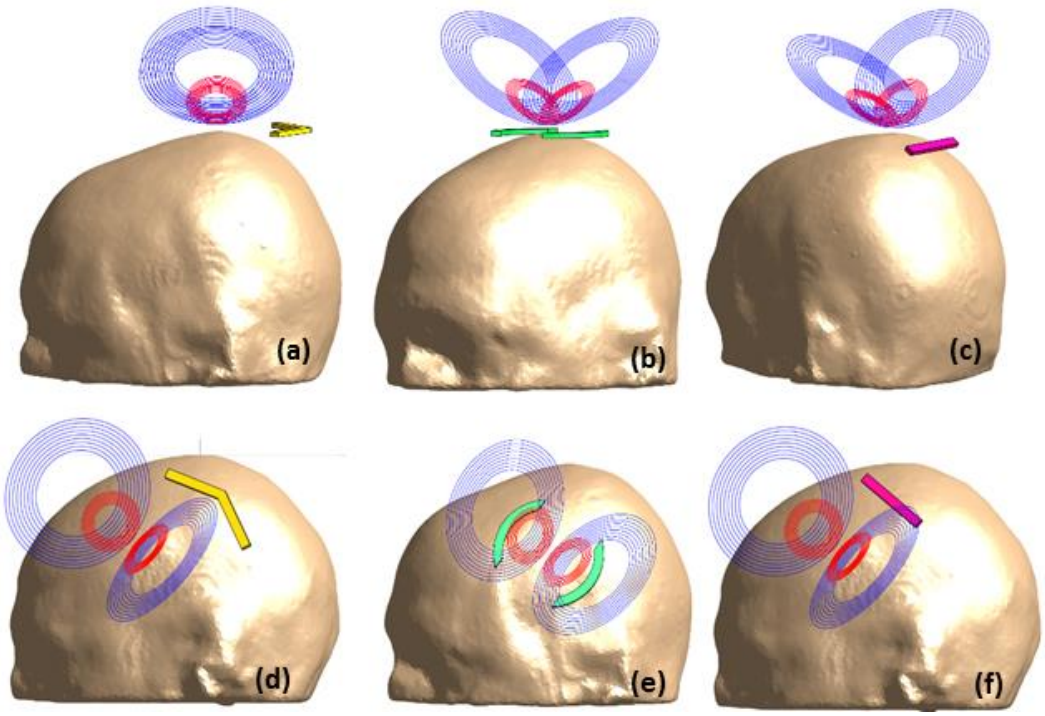

Figure 4-5. The shields position (a,d) V-shaped, (b,e) Two Semicircles (c,f) Brick, on the head model along with the QBC on the vertex and the dorsolateral prefrontal cortex position.

4.3.5 Dorsolateral prefrontal cortex

The shields discussed in section 4.3.4 were used in additional simulations over the DLPFC. This includes four more head models that have been chosen by a random number generator from the 50 head model set used in Rastogi *et al* [71]. It has been previously shown by the authors that the QBC with a shield has improvement in focality by 25% when compared with the conventional Magstim Figure-8 coil. In this dissertation, we have compared the simulation results using a QBC with and without the aforementioned coils. As presented in table 4-7, E-Max in GM &WM has increased due to the presence of three shields whilst E-Max (Entire Head) has decreased when the simulation was run without shields, at the vertex position. In addition, the stimulation with the QBC alone results in higher volume of stimulation and area of stimulation than when stimulating QBC with magnetic shield. The electric field ratio on

scalp to brain at the vertex for this head model is 2.12 for QBC alone, 1.80 for V-shape, 1.79 for Brick and 1.75 for Two Semicircles along with QBC.

Table 4-6: Shield dimensions and position.

Shield Shape	Position	Dimensions of the shield	Distance from the coil
V-shape	Vertex	Height: 3 mm Arm length: 40 mm Arm width: 6 mm Angle: 140°	57 mm from the center of the coil.
	Dorsolateral prefrontal cortex	Height: 3 mm Arm length: 40 mm Arm width: 6 mm Angle: 140°	50 mm from the Center of the coils. 2 mm below the plane of the coil.
Brick	Vertex	Length: 48 mm Width: 6 mm Height: 3 mm	36 mm from the center of the coils. 5 mm below the plane of the coil.
	Dorsolateral prefrontal cortex	Length: 48 mm Width: 6 mm Height: 3 mm	50 mm from the Center of the coils.
Two Semicircles	Vertex and Dorsolateral prefrontal cortex	Height: 3 mm Arc angle: 77.36° Width: 6 mm	3.5 mm (below the coil). Center of the arc and coil are right below each other.
	Dorsolateral prefrontal cortex	Height: 3 mm Arc angle: 77.36° Width: 6 mm	1.5 mm (below the coil). Center of the arc and coil are right below each other.

Table 4-7: Simulations results with three different shields.

Head Model	Shields	E-Max (GM &WM) V/m	E-Max (Entire Head) V/m	V-Half (GM &WM) m^3	A-Half (GM &WM) m^2
Head Model 1 at the vertex	Without shield	141.16	299.34	2.12E-06	7.84E-04
	V-shape	146.42	264.04	1.99E-06	7.83E-04
	Brick	147.54	264.05	2.00E-06	7.78E-04
	Two Semicircles	151.68	265.6	2.15E-06	8.38E-04
Average of 5 head models at the prefrontal	Without shield	145.38	287.46	6.76E-06	2.32E-03
	V-shape	152.50	204.84	4.33E-06	1.75E-03
	Brick	153.31	210.03	4.46E-06	1.79E-03
	Two Semicircles	167.91	237.94	4.69E-06	2.02E-03

We have shown simulation results in a total of five head models as researchers and clinicians are more interested in the dorsolateral prefrontal cortex than the vertex position[76]–[80]. When the coils were positioned at the vertex of the head the results showed trends similar to the trends observed in table 4-7. The electric field ratio between the scalp and brain at the dorsolateral prefrontal cortex for five head models is 1.98 for the QBC alone, 1.34 for V-shape, 1.37 for Brick and 1.42 for Two-Semicircles along with QBC which is very close to the Figure-8 (1.47). From these findings, it is clear that the focality has indeed been improved by the addition of magnetic shielding.

4.4 Conclusion

The first part of the chapter presents the use of magnetic shielding along with the QBC and compares the results with the original QBC and a Magstim 70 mm Figure-8 coil. The results were shown at two different locations over 50 heterogeneous head models. There is a modest,

yet significant improvement in focality when the QBC is used with a shield. Although, there is not much difference in the results of single and double shields with the QBC, both shielding solutions showed an improvement in focality of near 25% when compared to the conventional Magstim Figure-8 coil. Beyond brain stimulation, the improvements made to the relative intensity of scalp stimulation could also be an important factor for delivering TMS with greater patient tolerability.

Furthermore, it is clear that by changing the parameters such as thickness, distance, and permeability of the shielding material, show miniscule variation, but this could be due to the range of the values tested. This should be investigated further. Additionally, the researchers used a single model because the variation due to different shields was explored as opposed to the variation across many models. If the number of head models is increased, the variability among the models will make it difficult to isolate the effects of the shields alone. However, the results with one head model showed the same trend when tested with more models.

When the shields are within close proximity (approximately within 50 mm) to the coils, shifting the shield in any direction by 1cm, did not vary the results significantly. This result can be used to the researchers' advantage during clinical trials as head geometry varies with each person. Also, the shields used in this article or those used in the Rastogi *et al.* [71]were of small dimensions relative to the head and the coils. The reason smaller shields were selected is because they absorb less magnetic flux lines. Using bigger shields such as enclosed shields tends to absorb more magnetic flux lines and ultimately reduce the E-Max to values below 100 V/m. Furthermore, the use of magnetic shielding has displayed strong potential for improving the electric field ratio from scalp to brain and also to improve the E-Max and reduced the V-Half, thus improving the focality.

CHAPTER 5

INVESTIGATION OF COIL DESIGNS FOR SMALL ANIMAL

This chapter has used materials that were published in the paper "Investigation of Coil Designs for Transcranial Magnetic Stimulation on Mice", by P. Rastogi et. al, with the permission of all the authors [36].

5.1 Introduction

TMS studies on animals accelerate the development of treatments for deep brain disorders by reducing time, cost, and risk to humans. Although computational research on comparing TMS coils used for humans is widely reported, little is published on the use of different TMS coils on animals [27][81].

In this chapter, seven different TMS coil configurations were used for the stimulation on mouse brain are compared with electric and magnetic fields in different brain regions. This comparative study between the coil configurations will help the veterinarian and biomedical researchers working on mice to choose suitable coils according to their need, such as stimulating the brain with higher field or over small specific region of the brain.

5.2 Method

SEMCAD X, a finite element analysis tool, is used for the calculation of electric and magnetic fields inside the heterogeneous mouse model. Crowther et al. [82] have shown that the result from SEMCAD X modeling and measured magnetic field were in agreement. The mouse model was developed by the IT'IS Foundation [63][23].

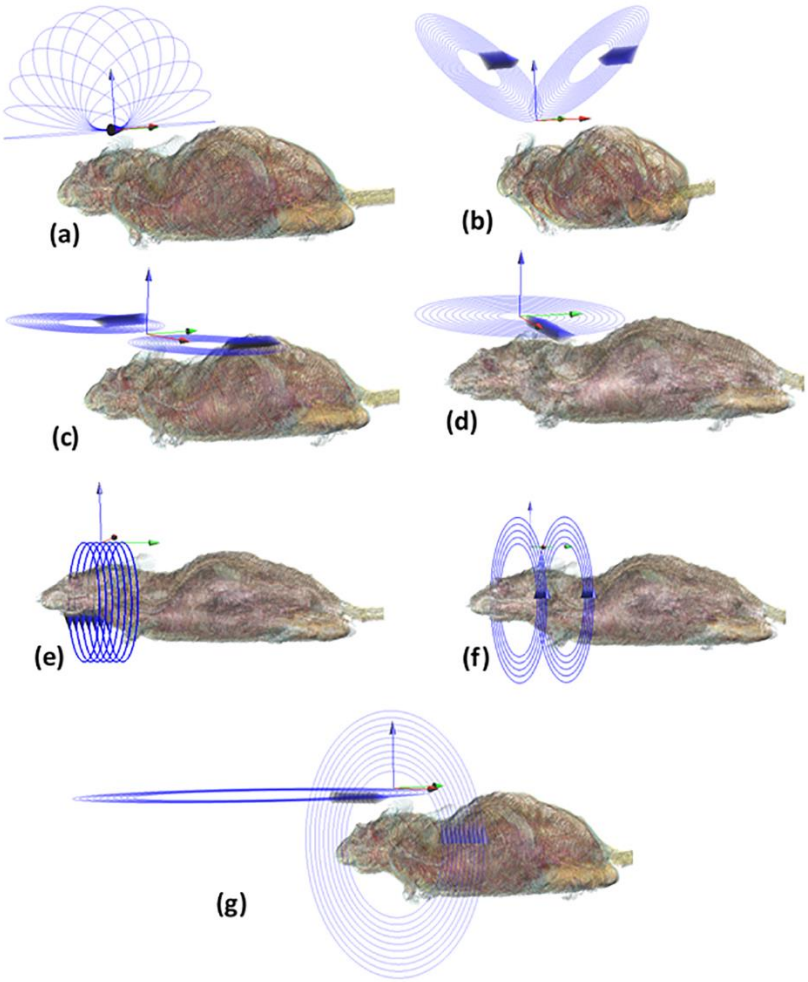

Figure 5-1. Different coil design configurations positioned on top of the heterogeneous mouse model (a) Slinky coil (b) "V" coil (c) Figure-of-8 coil (d) circular coil (e) solenoid coil (f) Helmholtz coil (g) Animal Halo coil.

This model was generated from MRI data of a male OF1 type mouse, with the body length of 95 mm (excluding tail) and weight of 35.5 gram and it consists of 50 different tissue layers such as skin, blood vessels, bone, and brain. Since these tissues were assigned corresponding electric and magnetic properties such as electric conductivity, magnetic permeability and relative permittivity at the operational frequency of 2.5 KHz, this mouse model gave accurate

results when compared to a homogenous mouse model or a homogenous sphere. All the coil configurations were given 5000 A current and tested at 100% output power. For accurate comparison with commercial coils, all the coils were kept at a distance of 5 mm from the highest point of the mouse head. At this position, the copper windings were placed at the same distance from the highest point of mouse head as the commercial coils, which have plastic insulation with a thickness of 5 mm (maximum value).

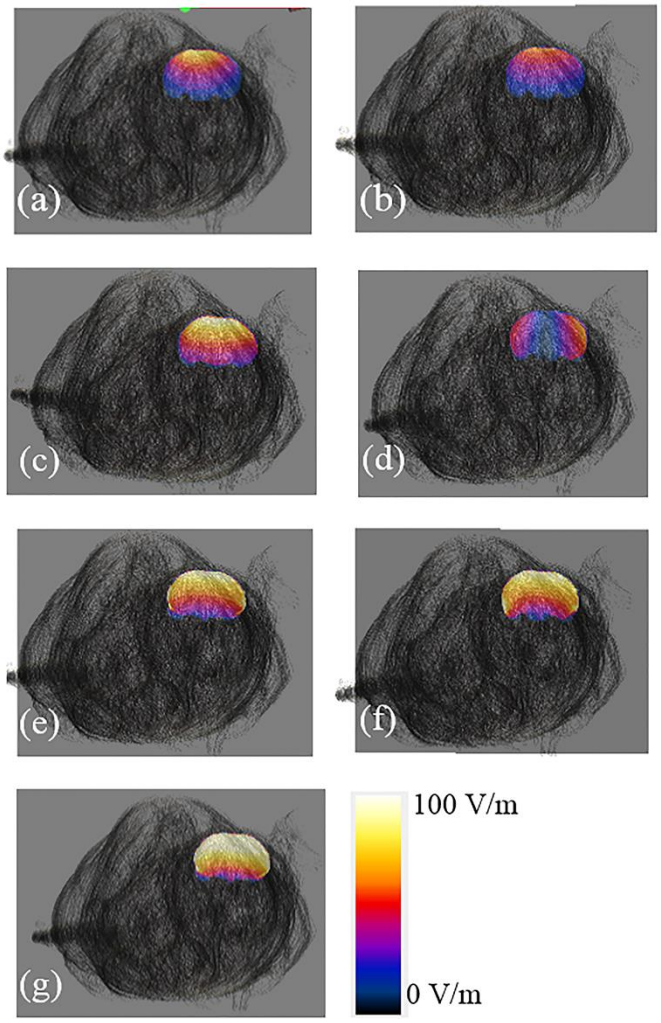

Figure 5-2. Coronal view of the induced electric field due to the (a) Slinky coil (b) "V" coil (c) Figure-of-8 coil (d) circular coil (e) solenoid coil (f) Helmholtz coil (g) Animal Halo Coil.

Deng et al. compared 50 different coil models on a homogeneous sphere and calculated depth and area of stimulation, whereas in this chapter, fewer number of coil models are used with a heterogeneous mouse model for more accurate electric and magnetic field calculation [37]. Fig. 5-1 shows seven different coil configurations which are compared in this paper: Slinky coil, "V" coil, Figure-of-8 coil, circular coil, solenoid coil, Helmholtz coil, and Animal Halo Coil.

Slinky coil, as shown in the Fig. 5-1(a) has 13 coils with the mean radius of 14 mm. The Figure-of-8 coil has two sets of coils with 15 coils in each of them, with the mean radius of 13 mm as seen in Fig. 5-1(c). "V" coil as illustrated in the Fig. 5-1(b) is similar to Figure-of-8 coil with the angle of 45 degree between the coils. The circular coil consists of 12 coils, with a mean radius of 16 mm which can be seen in Fig. 5-1(d). The solenoid coil has 10 coils with a radius of 20 mm as illustrated in Fig. 5-1(e). From Figure 1(f), we can see the Helmholtz coil with the total of 10 coils, divided in a group of two, and with the mean radius of 21 mm. Fig. 1(g) reveals the Animal Halo Coil with 10 coils in vertical position with a mean radius of 27 mm and 10 coils in horizontal position with a mean radius of 40 mm.

5.3 Results and Discussions

The magnetic and electric field profiles for each coil design have been calculated by finite element tool. The results have been compared due to variation in shape and size of TMS coils.

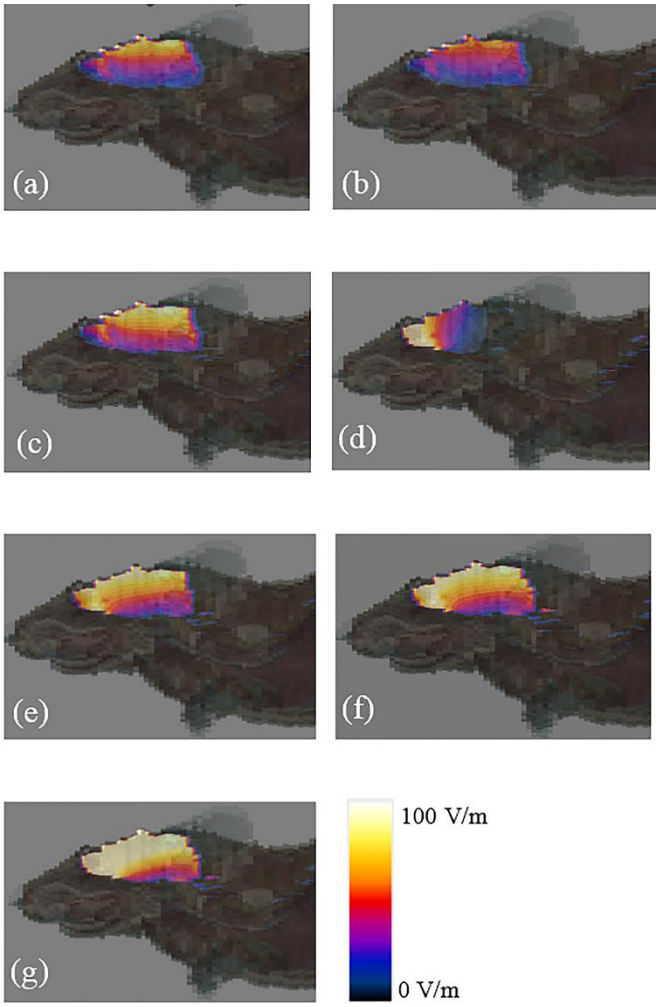

Figure 5-3. Sagittal view of the induced electric field due to the (a) Slinky coil (b) "V" coil (c) Figure-of-8 coil (d) circular coil (e) solenoid coil (f) Helmholtz coil (g) Animal Halo Coil.

Fig. 5-2 presents coronal view of the induced electric field inside the mouse brain, generated by different coil configurations. The scale for the induced electric field varies from 100 V/m to 0 V/m as shown by the color scale with dark color being zero field and bright color being the maximum field in the brain region. The red color in the color scale depicts electric field of approximately 50 V/m. It can be seen in Fig. 5-2 that the stimulation of the brain is different due to different coil configurations. The Slinky and "V" coil configuration stimulate the smallest region of the brain when compared to the other coil configurations (see Fig. 5-2(a)

& 5-2(b)). The induced electric field value was 100 V/m right below the coils and the rest of the region was 50 V/m or below. Fig. 5-2(d) reveals the induced electric field generated by the circular coil configuration, which stimulates the brain area away from the vertex of the brain unlike other coil configurations which stimulate directly beneath the coil on the vertex of the brain. This is due to the fact that the magnetic field is significantly smaller at the center of the circular coil and hence the induced electric field is less at the center of the mouse brain. Other coils such as Figure-of-8 coil, solenoid coil, and Helmholtz coil stimulate larger brain areas than the Slinky, V and circular coil configuration. The Animal Halo Coil configuration stimulates almost the entire mouse brain as presented in Fig. 5-2(g).

The sagittal view of the induced electric field in the mouse brain is shown in Fig. 5-3. The scale gradient of the induced electric field is kept same as in coronal view for better comparison of the results. Computer modelling reveals that only the outer layer of the brain is stimulated by the Slinky and "V" coil configuration illustrated in Fig. 5-3(a) & 5-3(b), whereas nearly half of the brain is stimulated by the Figure-of-8 coil configuration as shown in Fig. 5-3(c). The solenoid and Helmholtz coils stimulate nearly three quarters of the brain as revealed in Figures 5-3(e) & 5-3(f). Animal Halo Coil stimulates more than 90% of the brain as seen in Fig. 5-3(g).

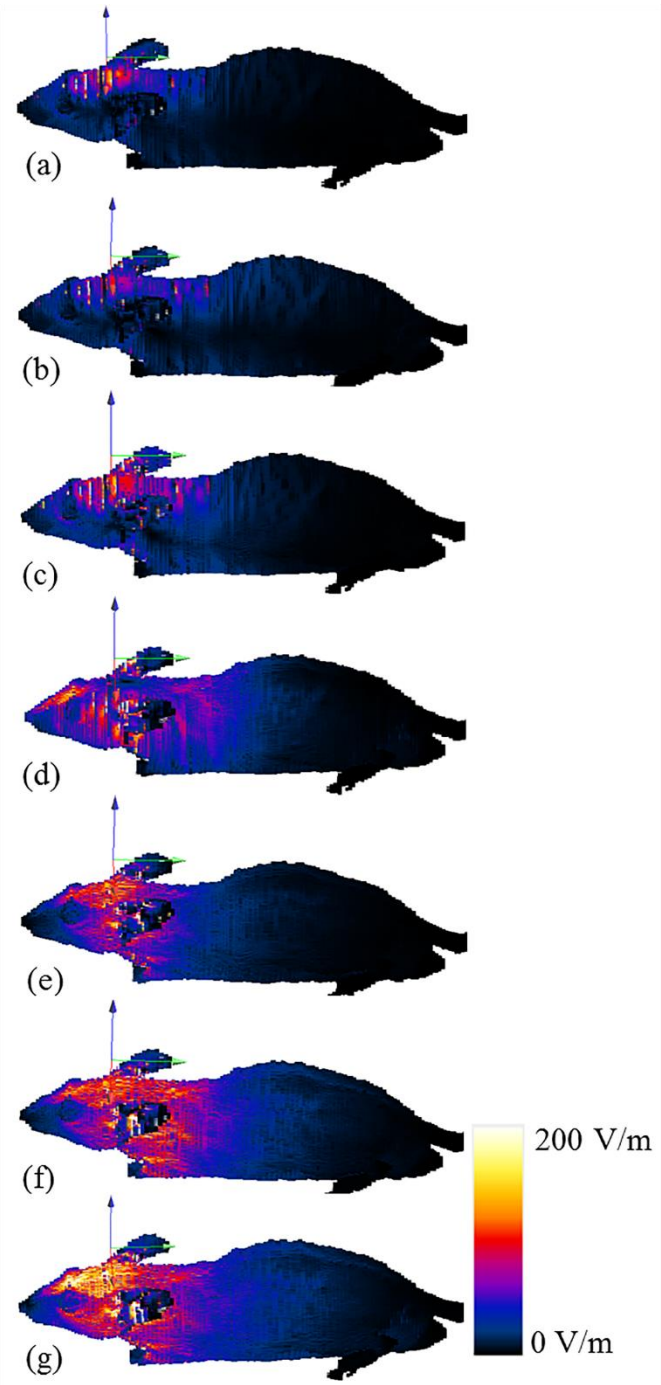

Figure 5-4. The surface electric field due to the coils (a) Slinky coil (b) "V" coil (c) Figure-of-8 coil (d) circular coil (e) solenoid coil (f) Helmholtz coil (g) Animal Halo Coil.

The coronal and sagittal view of the mouse brain gives the complete profile of the electrical field generated by each coil configurations. Fig. 5-4 shows the surface electric field on the mouse brain and on its body. The scale for the induced electric field is from 200 V/m to 0 V/m, which is different from the scale used in the previous images. It is shown by the color scale with dark color for zero field and bright color for the maximum field in the brain region. The red color in the color scale depicts the field value close to 100 V/m. Fig. 5-4 shows that the different coils have different surface electric field profiles. The slinky coil has the most focal electric field when compared to the other six coil configurations as presented in Fig. 5-4(a). The mouse body is not stimulated due to this coil configuration, a factor to be considered when other parts of the body such as neck or fore limbs are not to be stimulated. This means that this coil configuration is more advantageous than the other coils for experiments that require targeted stimulation. The area of stimulation is higher than for the Figure-of-8 coil when compared with the Slinky and "V" coil as shown in Fig. 5-4(c). Entire mouse head along with the neck is stimulated due to the size of the solenoid and Animal Halo Coil configuration.

Fig. 5-5 shows the magnetic field profile due to the different coil configurations on the mouse. The magnetic field is not affected by the tissue properties of the mouse as the value of permeability is approximately 1 in all the mouse tissues. The scale of the magnetic field is from 0 MA/m to 1 MA/m. Color scale is used for the scale where 0.5 MA/m is depicted by the red color. The magnetic field is 0.5 MA/m for half of the mouse brain generated by "Slinky" coil and "V" coil and covers the full brain when Figure-of-8 coil is used as seen in Fig. 5-5(a), 5-5(b) and 5-5(c).

Stimulation by circular coil is more than Figure-of-8 coil, where mouse neck is partially stimulated. The entire mouse head along with the neck is stimulated with the magnetic field

equal to or higher than 1 MA/m when stimulated by solenoid coil and Helmholtz coil as shown in Fig. 5-5 (e) and (f). Fig. 5-5(g) shows that the half of the mouse body is stimulated by magnetic field generated by Animal Halo Coil of 1 MA/m or more.

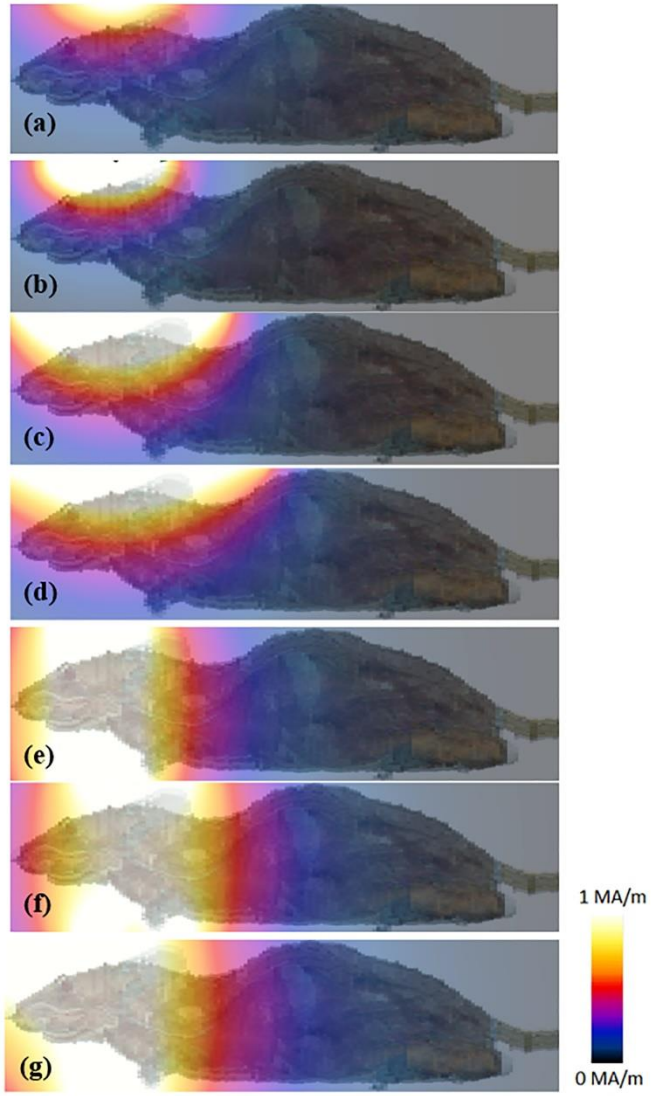

Figure 5-5. The magnetic field due to the coils (a) Slinky coil (b) "V" coil (c) Figure-of-8 coil (d) circular coil (e) solenoid coil (f) Helmholtz coil (g) Animal Halo Coil.

Table 5-1 lists the stimulated regions in the head by each coil configurations along with the depth of electric field above and equal to the threshold field needed to cause stimulation

(125 V/m) [68]. The table includes the stimulated regions such as skin, skull, cerebral hemisphere, olfactory, and cerebral spinal fluid in the mouse. In this paper, we have found that the Animal Halo Coil configuration has the maximum depth along with minimum focality. On the other hand, the Slinky coil has minimum depth with maximum focality. The depth of electric field due the Slinky coil is 1.5 mm, whereas that of electric field due to Animal Halo Coil is 9.2 mm.

Table 5-1. Stimulated regions and depth of the electric field for each coil configurations.

Coil Name	Stimulated Regions	Depth of electric field above and equal to 125 V/m
Slinky coil	Skin, skull and 1.5 mm of cerebral hemisphere from top of the head.	1.5 mm
"V" coil	Skin, skull and 1.5 mm of cerebral hemisphere from top of the head.	3.3 mm
Figure-of-8 coil	Skin, skull and 2.5 mm of cerebral hemisphere from the top (100 V/m for midbrain).	4.7 mm
circular coil	Skin, skull, olfactory bulb and 2 mm of cerebral hemisphere along the sagittal plane.	7.3 mm
solenoid coil	Skin, skull, cerebral hemisphere- 2.5 mm from top of the head and 1 mm from the sides, olfactory bulb and quarter of mid brain from top of the head.	8.1 mm
Helmholtz coil	Skin, skull, olfactory bulb, and half of the cerebral hemisphere.	8.3 mm
Animal Halo Coil	Skin, skull, cerebral hemisphere, olfactory bulb, region of cerebral spinal fluid close to the brain and three quarters of the mid brain from top of the head.	9.2 mm

5.4 Conclusion

Comparison of the different TMS coil configurations were conducted for the stimulation of a mouse brain. Electric and magnetic fields were calculated using a realistic heterogeneous mouse model when stimulated with different coil configurations such as “Slinky” coil, “V” coil, “Figure of Eight” coil, circular coil, solenoid coil, “Helmholtz” coil and “Animal Halo Coil”. It has been shown that the coil design plays an important role in the depth and area of stimulation of the mouse brain. Comparisons of these coils will help the veterinarians and biomedical researchers in finding suitable coils for treating particular neurological disorders in the mice.

CHAPTER 6

CONCLUSION AND FUTURE WORK

The work presented in this dissertation concerns the coil design amd development for the application of transcranial magnetic simulation (TMS). Two TMS coils namely the Triple Halo Coil and the Quadruple Butterfly Coil were presented, with one aiming for the deep brain stimulation and other one for spatially precise stimulation. For both the coils, computer modelling was done on heterogeneous head models using a finite element tool and testing using a prototype built by Jali Medical with the help of an axial Hall probe and a gaussmeter. Furthermore, several coil designs based on the magnitude of magnetic and induced electric field were discussed for small animals such of a mouse.

The TH coil is a TMS coil which is aimed for deep brain stimulation. It has improved depth of penetration of magnetic field due to this geometry and position with respect to the human brain. There are three set of elliptical coils in the TH coil, in which one coil is parallel to the ground and other two are at the angle of 30° with the first coil. The eccentricity of all the three coils is 0.74 and TH coil can be used with either Figure-8 coil or circular coil as the top coil. The magnetic field due to the TH coil is 7 times more than that of the circular coil at 10 cm below the head. It can stimulate deep brain regions which are affected in the disorders such as Parkinson's disease and PTSD. The induced electric field was calculated with the help of a heterogeneous head model. Furthermore, the TH coil prototype was fabricated and test results showed an excellent agreement between measured and calculated magnetic field at various locations.

Another coil QBC, which is also presented in this work, is a new coil with improved focality and comparable induced electric field with the Figure-8 coil. The QBC has four coils, two big and two small coils, where all are inclined at an angle of 90° to each other. The QBC has reduced volume of stimulation by around 10% at vertex and DLPFC when compared with the Figure-8 coil. Fifty heterogeneous MRI derived head models were used for the analysis of the induced electric field due to the QBC and the results were compared with the Figure-8 coil.

Passive magnetic shields of high permeabilities were used along with the QBC to further improve the focality. Parameters of interest such as permeability, position, thickness and shape of the magnetic shield were varied to further improve the precision due to the QBC. The QBC was also fabricated by Jali Medical and its magnetic field was measured using an axial Hall probe and gaussmeter. The QBC is suitable for the disorders in which precision is essential and required stimulating area is small. One of the potential application of QBC could be for therapeutic use in schizophrenia.

Furthermore, seven coils for small animals were presented in this dissertation. These coils had varying electric field with Slinky coil having the minimum area of stimulation and lowest electric field below 10 mm of the head, while Animal Halo Coil have maximum area of stimulation and highest electric field at 10 mm below the head. Animal coils are important as animal testing can reduce the cost and expedites research time.

The work presented in this dissertation concerns head modelling and coil designs. The work based on the head modelling could be expanded in various ways such as increasing the segmentations of the head models, improving the resolution, including fiber tracks data, having head models of patients with specific disorders and creating head models of patients with

clinical data on TMS. Coil design can always be further improved by working on the new coil geometry having focality or deep brain stimulation or improving the current ones.

The coil development presented in this dissertation can be explored with different positions on the head, targeting specific disorders such as investigating the QBC at auditory cortex which is related to the schizophrenia. Furthermore, MRI head models can be developed which also have the clinical data for a specific disorder and then both the computer simulation and clinical data can be compared. The passive shields used along with QBC can be manufactured and they can be tested along the coil. Both the QBC and TH coil can be further improved in order to increase the electric field and reduce the volume of stimulation.

REFERENCES

[1] "WHO | Mental disorders affect one in four people," *WHO*, 2013.

[2] "NIMH » Major Depression Among Adults." [Online]. Available: https://www.nimh.nih.gov/health/statistics/prevalence/major-depression-among-adults.shtml. [Accessed: 16-Nov-2017].

[3] NIMH, "Schizophrenia." [Online]. Available: https://www.nimh.nih.gov/health/statistics/schizophrenia.shtml. [Accessed: 02-Jul-2018].

[4] NIMH, "Post-Traumatic Stress Disorder (PTSD)." [Online]. Available: https://www.nimh.nih.gov/health/statistics/post-traumatic-stress-disorder-ptsd.shtml. [Accessed: 03-Jul-2018].

[5] NIH, "NIH Fact Sheets - Parkinson's Disease." [Online]. Available: https://report.nih.gov/NIHfactsheets/ViewFactSheet.aspx?csid=109. [Accessed: 06-Aug-2018].

[6] J. Greenhalgh, C. Knight, D. Hind, C. Beverley, and S. Walters, "Clinical and cost-effectiveness of electroconvulsive therapy for depressive illness, schizophrenia, catatonia and mania: systematic reviews and economic modelling studies.," *Health Technol. Assess.*, vol. 9, no. 9, Mar. 2005.

[7] M. Seshadri and N. Z. Mazi-kotwal, "Response Predictors in ECT: A discussion about Seizure Threshold | British Journal of Medical Practitioners," *BJMP*, 2011. [Online]. Available: http://www.bjmp.org/content/response-predictors-ect-discussion-about-seizure-threshold. [Accessed: 25-May-2016].

[8] R. Eitan and B. Lerer, "Nonpharmacological, somatic treatments of depression: electroconvulsive therapy and novel brain stimulation modalities.," *Dialogues Clin. Neurosci.*, vol. 8, no. 2, pp. 241–58, Jan. 2006.

[9] M. A. Nitsche and W. Paulus, "Excitability changes induced in the human motor cortex by weak transcranial direct current stimulation," *J. Physiol.*, vol. 527, no. 3, pp. 633–639, Sep. 2000.

[10] R. H. Howland, "Vagus Nerve Stimulation.," *Curr. Behav. Neurosci. reports*, vol. 1, no. 2, pp. 64–73, Jun. 2014.

[11] J. C. Horvath, J. M. Perez, L. Forrow, F. Fregni, and A. Pascual-Leone, "Transcranial magnetic stimulation: a historical evaluation and future prognosis of therapeutically relevant ethical concerns," *J. Med. Ethics*, 2010.

[12] D. M. Wegner, *The illusion of conscious will*, Illustrate. MIT Press, 2017.

[13] A. Pascual-Leone, J. Valls-Solé, E. M. Wassermann, and M. Hallett, "Responses to rapid-rate transcranial magnetic stimulation of the human motor cortex," *Brain*, vol. 117, no. 4, pp. 847–858, Aug. 1994.

[14] A. Pascual-Leone, J. R. Gates, and A. Dhuna, “Induction of speech arrest and counting errors with rapid-rate transcranial magnetic stimulation.,” *Neurology*, vol. 41, no. 5, pp. 697–702, May 1991.

[15] S. Ueno, T. Tashiro, and K. Harada, “Localized stimulation of neural tissues in the brain by means of a paired configuration of time-varying magnetic fields,” *J. Appl. Phys.*, vol. 64, no. 10, p. 5862, 1988.

[16] H. M. Kolbinger, G. Höflich, A. Hufnagel, H.-J. Müller, and S. Kasper, “Transcranial magnetic stimulation (TMS) in the treatment of major depression — a pilot study,” *Hum. Psychopharmacol. Clin. Exp.*, vol. 10, no. 4, pp. 305–310, Jul. 1995.

[17] J. Selvaraj, P. Rastogi, N. P. Gaunkar, R. L. Hadimani, and M. Mina, “Transcranial Magnetic Stimulation: Design of a Stimulator and a Focused Coil for the Application of Small Animals,” *IEEE Trans. Magn.*, pp. 1–5, 2018.

[18] Magstim, “Magstim - Heritage.” [Online]. Available: https://www.magstim.com/heritage. [Accessed: 19-Aug-2018].

[19] Neuronetics, “About Us - Company Profile, Corporate History | NeuroStar.” [Online]. Available: https://neurostar.com/neuronetics/. [Accessed: 19-Aug-2018].

[20] Magventure, “Our history.” [Online]. Available: https://www.magventure.com/about-us/our-history. [Accessed: 19-Aug-2018].

[21] Brainsway, “About Us - Brainsway.” [Online]. Available: https://www.brainsway.com/about-us/. [Accessed: 19-Aug-2018].

[22] P. I. Williams, P. Marketos, L. J. Crowther, and D. C. Jiles, “New designs for deep brain transcranial magnetic stimulation,” *IEEE Trans. Magn.*, vol. 48, no. 3, pp. 1171–1178, 2012.

[23] IT’IS Foundation, “Virtual Population.” [Online]. Available: http://www.itis.ethz.ch/virtual-population/virtual-population-cvip-vip/overview/. [Accessed: 13-Oct-2015].

[24] A. T. Barker, R. Jalinous, and I. L. Freeston, “Non-Invasive Magnetic Stimualtion Of Human Motor Cortex,” *The Lancet*, vol. 325, no. 8437. Elsevier, pp. 1106–1107, May-1985.

[25] A. Nummenmaa *et al.*, “Targeting of White Matter Tracts with Transcranial Magnetic Stimulation,” *Brain Stimul.*, vol. 7, pp. 80–84, 2014.

[26] A. Opitz, M. D. Fox, R. C. Craddock, S. Colcombe, and M. P. Milham, “An integrated framework for targeting functional networks via transcranial magnetic stimulation,” *Neuroimage*, vol. 127, pp. 86–96, 2016.

[27] S. D. March *et al.*, “Focused and deep brain magnetic stimulation using new coil design in mice,” in *2013 6th International IEEE/EMBS Conference on Neural Engineering (NER)*, 2013, pp. 125–128.

[28] Y. Meng, R. L. Hadimani, L. J. Crowther, Z. Xu, J. Qu, and D. C. Jiles, “Deep brain

transcranial magnetic stimulation using variable ‘Halo coil’ system,” *J. Appl. Phys.*, vol. 117, no. 17, p. 17B305, May 2015.

[29] J. Downar and Z. J. Daskalakis, “New Targets for rTMS in Depression: A Review of Convergent Evidence,” *Brain Stimul.*, vol. 6, pp. 231–240, 2013.

[30] A. Suppa *et al.*, “Ten Years of Theta Burst Stimulation in Humans: Established Knowledge, Unknowns and Prospects,” *Brain Stimul.*, vol. 9, pp. 323–335, 2016.

[31] A. V. Peterchev, R. Jalinous, and S. H. Lisanby, “A Transcranial Magnetic Stimulator Inducing Near-Rectangular Pulses With Controllable Pulse Width (cTMS),” *IEEE Trans. Biomed. Eng.*, vol. 55, no. 1, pp. 257–266, Jan. 2008.

[32] C. C. Cline, N. N. Johnson, and Bin He, “Subject-specific optimization of channel currents for multichannel transcranial magnetic stimulation,” in *2015 37th Annual International Conference of the IEEE Engineering in Medicine and Biology Society (EMBC)*, 2015, pp. 2083–2086.

[33] S. M. Goetz, D. L. K. Murphy, and A. V. Peterchev, “Transcranial Magnetic Stimulation Device With Reduced Acoustic Noise,” *IEEE Magn. Lett.*, vol. 5, pp. 1–4, 2014.

[34] L. L. Carpenter *et al.*, “rTMS with a two-coil array: Safety and efficacy for treatment resistant major depressive disorder,” 2017.

[35] L. M. Koponen, J. O. Nieminen, T. P. Mutanen, M. Stenroos, and R. J. Ilmoniemi, “Coil optimisation for transcranial magnetic stimulation in realistic head geometry,” 2017.

[36] P. Rastogi, R. L. Hadimani, and D. C. Jiles, “Investigation of Coil Designs for Transcranial Magnetic Stimulation on Mice,” *IEEE Trans. Magn.*, vol. 52, no. 7, pp. 1–4, Jul. 2016.

[37] Z.-D. Deng, S. H. Lisanby, and A. V Peterchev, “Electric field depth-focality tradeoff in transcranial magnetic stimulation: simulation comparison of 50 coil designs.,” *Brain Stimul.*, vol. 6, no. 1, pp. 1–13, Jan. 2013.

[38] V. Guadagnin, M. Parazzini, S. Fiocchi, I. Liorni, and P. Ravazzani, “Deep Transcranial Magnetic Stimulation: Modeling of Different Coil Configurations,” *IEEE Trans. Biomed. Eng.*, vol. 63, no. 7, pp. 1543–1550, Jul. 2016.

[39] Z.-D. Deng, S. H. Lisanby, and A. V. Peterchev, “Coil design considerations for deep transcranial magnetic stimulation,” *Clin. Neurophysiol.*, vol. 125, no. 6, pp. 1202–1212, 2014.

[40] A. Zangen, Y. Roth, B. Voller, and M. Hallett, “Transcranial magnetic stimulation of deep brain regions: evidence for efficacy of the H-coil.,” *Clin. Neurophysiol.*, vol. 116, no. 4, pp. 775–9, Apr. 2005.

[41] L. J. Crowther, P. Marketos, P. I. Williams, Y. Melikhov, D. C. Jiles, and J. H. Starzewski, “Transcranial magnetic stimulation: Improved coil design for deep brain investigation,” *J. Appl. Phys.*, vol. 109, no. 7, pp. 2009–2012, 2011.

[42] E. V. Harel, A. Zangen, Y. Roth, I. Reti, Y. Braw, and Y. Levkovitz, "H-coil repetitive transcranial magnetic stimulation for the treatment of bipolar depression: an add-on, safety and feasibility study," *World J. Biol. Psychiatry*, vol. 12, no. 2, pp. 119–126, Mar. 2011.

[43] S. Fiocchi, M. Parazzini, I. Liorni, Y. Roth, A. Zangen, and P. Ravazzani, "Deep transcranial magnetic stimulation for the treatment of neuropsychiatric disorders in elderly people: Electric field assessment," in *2015 International Conference on Electromagnetics in Advanced Applications (ICEAA)*, 2015, pp. 448–451.

[44] Y. Roth, A. Amir, Y. Levkovitz, and A. Zangen, "Three-Dimensional Distribution of the Electric Field Induced in the Brain by Transcranial Magnetic Stimulation Using Figure-8 and Deep H-Coils," *J. Clin. Neurophysiol.*, vol. Volume 24, no. issue 1, p. pp 31-38.

[45] P. Rastogi, E. G. Lee, R. L. Hadimani, and D. C. Jiles, "Transcranial Magnetic Stimulation: Development of a Novel Deep-Brain Triple-Halo Coil," *IEEE Magn. Lett.*, vol. 10, pp. 1–5, 2019.

[46] R. Cantello, "Transcranial magnetic stimulation and Parkinson's disease," *Brain Res. Rev.*, vol. 38, no. 3, pp. 309–327, Feb. 2002.

[47] Schmid & Partner Engineering AG, "SEMCAD X." [Online]. Available: http://www.speag.com/products/semcad/intro/. [Accessed: 11-Sep-2015].

[48] E. Neufeld, M. C. Gosselin, D. Sczcerba, M. Zefferer, and N. Kuster, "Sim4Life: A Medical Image Data Based Multiphysics Simulation Platform for Computational Life Sciences," *Proc. VPH 2012 Congr. 2012)*, 2012.

[49] M.-C. Gosselin *et al.*, "Development of a new generation of high-resolution anatomical models for medical device evaluation: the Virtual Population 3.0," *Phys. Med. Biol.*, vol. 59, no. 18, pp. 5287–5303, 2014.

[50] A. Christ *et al.*, "The Virtual Family - development of surface-based anatomical models of two adults and two children for dosimetric simulations," *Phys. Med. Biol.*, vol. 55, no. 2, pp. N23–N38, 2010.

[51] "Magstim." [Online]. Available: https://www.magstim.com/. [Accessed: 03-Nov-2017].

[52] P. Rastogi, Y. Tang, B. Zhang, E. G. Lee, R. L. Hadimani, and D. C. Jiles, "Quadruple Butterfly Coil with Passive Magnetic Shielding for Focused Transcranial Magnetic Stimulation," *IEEE Trans. Magn.*, pp. 1–1, 2017.

[53] P. Rastogi, B. Zhang, Y. Tang, E. G. Lee, R. L. Hadimani, and D. C. Jiles, "Investigation of shape, position, and permeability of shielding material in quadruple butterfly coil for focused transcranial magnetic stimulation," *AIP Adv.*, vol. 8, no. 5, p. 056705, May 2018.

[54] G. Deuschl *et al.*, "A Randomized Trial of Deep-Brain Stimulation for Parkinson's Disease," *N. Engl. J. Med.*, vol. 355, no. 9, pp. 896–908, Aug. 2006.

[55] S. Ueno, T. Matsuda, and M. Fujiki, “Functional mapping of the human motor cortex obtained by focal and vectorial magnetic stimulation of the brain,” *IEEE Trans. Magn.*, vol. 26, no. 5, pp. 1539–1544, 1990.

[56] J. C. Horvath, J. Mathews, M. A. Demitrack, and A. Pascual-Leone, “The NeuroStar TMS device: conducting the FDA approved protocol for treatment of depression.,” *J. Vis. Exp.*, no. 45, 2010.

[57] Magstim, “Magstim - Magstim Announces FDA (510k) Clearance of rTMS (repetitive Transcranial Magnetic Stimulation) Therapy System.” [Online]. Available: http://www.magstim.com/article/13/magstim-announces-fda-510k-clearance-of-rtms-repetitive-transcranial-magnetic-stimulation-therapy-system. [Accessed: 22-Sep-2016].

[58] MagVenture, “MagVenture.” [Online]. Available: http://www.magventure.com/en-gb/. [Accessed: 22-Sep-2016].

[59] E. V. Harel, L. Rabany, L. Deutsch, Y. Bloch, A. Zangen, and Y. Levkovitz, “H-coil repetitive transcranial magnetic stimulation for treatment resistant major depressive disorder: An 18-week continuation safety and feasibility study,” *World J. Biol. Psychiatry*, vol. 15, no. 4, pp. 298–306, May 2014.

[60] E. G. Lee *et al.*, “Investigational Effect of Brain-Scalp Distance on the Efficacy of Transcranial Magnetic Stimulation Treatment in Depression,” *IEEE Trans. Magn.*, vol. 52, no. 7, pp. 1–4, Jul. 2016.

[61] D. C. Van Essen *et al.*, “The Human Connectome Project: A data acquisition perspective,” *Neuroimage*, vol. 62, no. 4, pp. 2222–2231, Oct. 2012.

[62] M. Windhoff, O. Alexander, and T. Axel, “Electric field calculations in brain stimulation based on finite elements: An optimized processing pipeline for the generation and usage of accurate individual head models,” *Hum. Brain Mapp.*, vol. 34, no. 4, pp. 923–935, 2013.

[63] P. A. Hasgall *et al.*, “IT’IS Database for thermal and electromagnetic parameters of biological tissues,” 2015. [Online]. Available: www.itis.ethz.ch/database.

[64] Magstim, “70mm double coil.” [Online]. Available: http://www.magstim.com/products/coils.

[65] F. Maeda, J. P. Keenan, J. M. Tormos, H. Topka, and A. Pascual-Leone, “Interindividual variability of the modulatory effects of repetitive transcranial magnetic stimulation on cortical excitability.,” *Exp. brain Res.*, vol. 133, no. 4, pp. 425–30, Aug. 2000.

[66] J. A. Kleim *et al.*, “BDNF val66met polymorphism is associated with modified experience-dependent plasticity in human motor cortex.,” *Nat. Neurosci.*, vol. 9, no. 6, pp. 735–7, Jun. 2006.

[67] H. Eaton, “Electric field induced in a spherical volume conductor from arbitrary coils: application to magnetic stimulation and MEG.,” *Med. Biol. Eng. Comput.*, vol. 30, no. 4, pp. 433–40, Jul. 1992.

[68] M. Lu and S. Ueno, “Deep Transcranial Magnetic Stimulation Using Figure-of-Eight and Halo Coils,” *IEEE Trans. Magn.*, vol. 9464, no. c, pp. 1–1, 2015.

[69] L. J. Crowther, “Analysis and development of transcranial magnetic stimulation devices,” *Grad. Theses Diss.*, vol. 14088, 2014.

[70] J. J. Borckardt *et al.*, “Reducing Pain and Unpleasantness During Repetitive Transcranial Magnetic Stimulation,” *J. ECT*, vol. 22, no. 4, pp. 259–264, Dec. 2006.

[71] P. Rastogi, E. G. Lee, R. L. Hadimani, and D. C. Jiles, “Transcranial Magnetic Stimulation-coil design with improved focality,” *AIP Adv.*, vol. 7, no. 5, p. 056705, May 2017.

[72] S. Ueno, T. Tashiro, and K. Harada, “Localized stimulation of neural tissues in the brain by means of a paired configuration of time-varying magnetic fields,” *J. Appl. Phys.*, vol. 64, no. 10, p. 5862, 1988.

[73] A. Pascual-Leone, B. Rubio, F. Pallardó, and M. D. Catalá, “Rapid-rate transcranial magnetic stimulation of left dorsolateral prefrontal cortex in drug-resistant depression,” *Lancet*, vol. 348, no. 9022, pp. 233–237, Jul. 1996.

[74] D. H. Kim, G. E. Georghiou, and C. Won, “Improved field localization in transcranial magnetic stimulation of the brain with the utilization of a conductive shield plate in the stimulator,” *IEEE Trans. Biomed. Eng.*, vol. 53, no. 4, pp. 720–725, 2006.

[75] I. Laakso and A. Hirata, “Reducing the staircasing error in computational dosimetry of low-frequency electromagnetic fields,” *Phys. Med. Biol.*, vol. 57, no. 4, pp. N25–N34, Feb. 2012.

[76] M. Kobayashi and A. Pascual-Leone, “Transcranial magnetic stimulation in neurology,” *Lancet Neurol.*, vol. 2, no. 3, pp. 145–156, 2003.

[77] P. B. Fitzgerald, S. Fountain, and Z. J. Daskalakis, “A comprehensive review of the effects of rTMS on motor cortical excitability and inhibition,” *Clin. Neurophysiol.*, vol. 117, no. 12, pp. 2584–2596, 2006.

[78] H. Siebner and J. Rothwell, “Transcranial magnetic stimulation: new insights into representational cortical plasticity,” *Exp. Brain Res.*, vol. 148, no. 1, pp. 1–16, Jan. 2003.

[79] M. T. K. Kirkcaldie, S. A. Pridmore, and A. Pascual-Leone, “Transcranial magnetic stimulation as therapy for depression and other disorders.,” *Aust. N. Z. J. Psychiatry*, vol. 31, no. 2, pp. 264–272, 1997.

[80] C. Hovey and R. Jalinous, “The guide to magnetic stimulation,” 2006.

[81] S. D. March *et al.*, “Thermal and Mechanical Analysis of Novel Transcranial Magnetic Stimulation Coil for Mice,” *IEEE Trans. Magn.*, vol. 50, no. 9, pp. 1–5, 2014.

[82] L. J. Crowther, R. L. Hadimani, a. G. Kanthasamy, and D. C. Jiles, “Transcranial magnetic stimulation of mouse brain using high-resolution anatomical models,” *J.*

Appl. Phys., vol. 115, no. 17, pp. 17–20, 2014.